Light Stable Isotopes in Volcanic-Hosted Massive Sulfide Ore Systems

David L. Huston, Crystal Laflamme, Georges Beaudoin, and Stephen Piercey

Abstract

Volcanic-hosted massive sulfide (VHMS) deposits, the ancient analogues of "black smoker" deposits that currently form on the seafloor, are the products of complex mineral systems involving the interaction of seawater with the underlying volcanic pile and associated magmatic intrusions. Light stable isotopes, particularly those of oxygen, hydrogen and sulfur, have had a strong influence in determining sources of ore fluids and sulfur as well as elucidating geological processes important in the VHMS mineral systems. Oxygen and hydrogen isotope data indicate that evolved seawater was the dominant ore-forming fluid in VHMS mineral systems through geological time, although a small proportion of deposits, including high sulfidation and tin-rich deposits, may have a significant, or dominant, magmatic-hydrothermal fluid component. Higher-temperature (> 200 °C) interaction of evolved seawater alters the rock pile below the seafloor, producing $\delta^{18}O$ depletion anomalies at the deposit and district scales that can be used as a vector to ore. In contrast, lower-temperature hydrothermal alteration results in $\delta^{18}O$-enriched zones that commonly cap mineralized positions. An apparent decrease in the degree of high temperature ^{18}O depletion with time may relate to the increasing importance of felsic-dominated host successions in younger deposits. $\delta^{18}O$ anomalies have potential as an exploration tool, and have contributed directly to discovery. The other important contribution of stable isotopes to understanding the VHMS mineral system is quantification of the contribution of sulfur sources. Conventional $\delta^{34}S$ data, when combined with $\Delta^{33}S$ data acquired using recently developed technologies, indicate that the dominant sulfur source is igneous sulfur, either leached from the volcanic pile or introduced as a magmatic volatile (these sources are not distinguishable). The thermochemical reduction of seawater sulfate is also an important, but subordinate, sulfur source.

Supplementary Information The online version contains supplementary material available at https://doi.org/10.1007/978-3-031-27897-6_9.

D. L. Huston (✉)
Geoscience Australia, GPO Box 378, Canberra, ACT 2601, Australia
e-mail: David.Huston@ga.gov.au

C. Laflamme · G. Beaudoin
Département de Géologie Et de Génie Géologique, Centre de Recherche Sur La Géologie Et L'ingénierie Des Ressources Minérales (E4m), Université Laval, 1065, Avenue de La Médecine, Québec, QC G1V 0A6, Canada

S. Piercey
Department of Earth Sciences, Memorial University of Newfoundland, Room 4063, Alexander Murray Building, 9 Arctic Avenue, St. John's, NL 1B 3X5, Canada

D. Huston and J. Gutzmer (eds.), *Isotopes in Economic Geology, Metallogenesis and Exploration*, Mineral Resource Reviews, https://doi.org/10.1007/978-3-031-27897-6_9

Estimation of the proportion of seawater sulfate with geological age indicate that, on average, it has increased from 5–10% in the Archean to 20–25% in the Phanerozoic. This most likely reflects the increase in seawater sulfate contents through geological time. Although untested as an exploration tool, variations in sulfur isotope data may have utility is discriminating fertile from barren sulfide accumulations or providing vectors to ores at the deposits scale. As exploration tools, light stable isotopes suffer from a relatively high cost and slow turn-around time. If these limitations can be overcome, and new analytical methods can be developed, light stable isotopes may emerge as another tool for exploration, particularly as discoveries are made at greater depth and under cover.

1 Introduction

As discussed elsewhere in this volume, light stable isotope data has proven key to understanding the genesis of a range of mineral systems (Hagemann et al. 2023; Huston et al. 2023; Quesnel et al. 2023; Williams 2023). Although these data have been particularly useful in understanding the sources of ore fluids and sulfur, the data also have proven useful in exploration (Miller et al. 2001). This chapter presents an overview of variations in stable isotope geochemistry in the volcanic-hosted massive sulfide (VHMS) mineral system and how this data has been used to understand this system and where it may be practical for exploration vectoring. It follows and builds on previous syntheses of stable isotopes in VHMS systems by Huston (1999), Shanks (2014) and Leybourne et al. (2022) and of active seafloor systems by Zierenberg and Shanks (1988) and Shanks (2001). Studies of active systems provide information such as direct isotopic measurements of venting fluids and the effect of changes during the timespan of the mineral system not available from studies of ancient systems.

2 The Volcanic-hosted Massive Sulfide Mineral System

The VHMS mineral system is arguably one of the best documented and understood mineral system. As VHMS deposits are preserved in many different parts of the world and formed through much of Earth's history, they provide, collectively, information on geological processes through time, including changes in hydrothermal and environmental processes. Despite these changes, VHMS deposits through time share many characteristics, both at the deposit- and district- to province-scale.

The understanding of the VHMS mineral system has come about not only from ancient deposits (Franklin et al. 1981, 2005; Huston et al. 2006) but also the discovery of "black smoker" deposits in modern oceanic basins (e.g., Hannington et al. 2005), which are thought to be modern analogues of VHMS deposits. Currently, hydrothermal fluids circulate extensively through the upper crust, particularly in submarine extensional zones associated with mid-oceanic ridges on divergent margins, or back-arc basins/rifted arcs along convergent margins. This circulation not only cools the oceanic upper crust, controlling the Earth's surficial heat budget (Stein 1995), but the fluids leach metals from the underlying rock and transfer these metals into the hydrosphere, having a major impact on the seawater metal budget. Although most metal is lost to the seawater column when these fluids vent (Converse et al. 1984), some of the metal is trapped in massive sulfide deposits that form at or just below the seafloor at venting sites (Herzig and Hannington 1995); the vents are also sites of abundant biological activity (Hannington et al. 2011). The growth of seafloor massive sulfide deposits involves dissolution, alteration and replacement of rock and massive sulfide within and below the mounds, forming complex mixtures of sulfide and altered host rock known as stockworks (Petersen et al. 2018).

Studies indicate that geologically ancient VHMS deposits formed mostly in back-arc

basins and rifted arcs along convergent margins (e.g., Franklin et al. 2005). This differs from modern black smokers, which are known to form along both mid-oceanic ridges as well as back-arc basins and rifted arcs (Hannington et al. 2005). This difference arises due the low likelihood of preserving oceanic crust in the ancient record—most of this crust is lost to subduction. Figure 1 illustrates an idealized asymmetric, VHMS-bearing back-arc basin that has rifted pre-existing continental crust to the left and an arc that developed on this crust to the right. Geochemical analyses of volcanic successions that host VHMS deposits (Lesher et al., 1986; Kerrich and Wyman 1997; Hart et al. 2004; Piercey 2011) indicate that both back-arc and arc signatures are present in VHMS districts.

Volcanism and the associated magmatism are integral components of the VHMS mineral system, providing heat, fluids, metals and/or sulfur. The left-hand side of Fig. 1 illustrates a VHMS system associated with a semi-conformable, subvolcanic intrusion that has provided heat to drive fluid flow. The associated volcanic pile provided metals and sulfur to the mineralizing fluids. The right-hand side illustrates a situation in which a cross-cutting intrusion, possibly arc-related, has provided heat, metals, sulfur and fluids to the evolving VHMS system. These two systems should be considered end-member variants of the VHMS mineral system.

The other major source of system components in VHMS systems is the overlying seawater column. Based mostly on stable isotope evidence seawater is thought to be the dominant fluid source in most VHMS systems and an important source of sulfur in many, particularly younger, systems. The left-hand inset in Fig. 1 illustrates a mineral system in which emplacement of a semi-conformable, subvolcanic intrusion (c.f. Galley 2003) at a depth of 3–5 km drives convection of seawater in the volcanic pile. This produces semi-conformable alteration zones above the intrusion that become cross-cutting along syn-volcanic structures to become the proximal alteration zones associated with most VHMS deposits. This alteration pattern records the convection of evolving seawater that interacts with

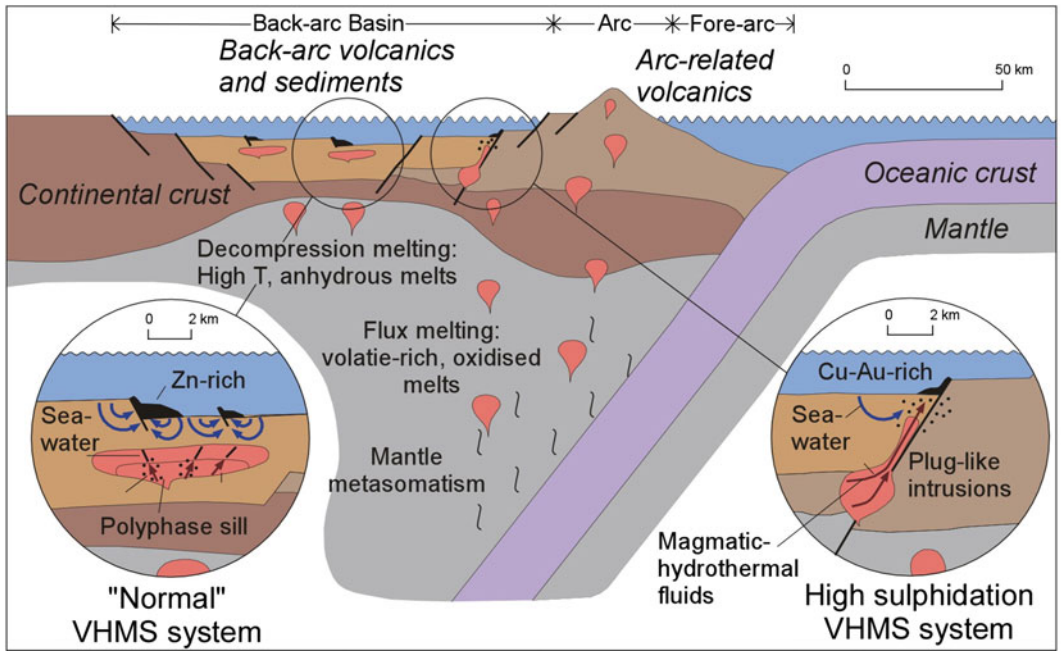

Fig. 1 Volcanic-hosted massive sulfide mineral system. Reproduced with permission from Huston et al. (2011); Copyright 2011 Geoscience Australia

the volcanic pile to extract metal and sulfur then moves upwards through the pile and deposits sulfur and metals to form a VHMS deposit. If the seawater was sulfate-bearing, reduction to sulfide by high temperature water–rock interaction was a second source of sulfur in the system.

Volcanic-hosted massive sulfide deposits form at and just below the seafloor and comprise three types of mineralized rock, stockwork, massive sulfide and exhalite (Fig. 2; Franklin et al. 1981, 2005; Huston et al. 2006). The stockwork zone consists of anastomosing veins, or "stockworks", of sulfide-bearing veins that also commonly contain quartz, carbonate, chlorite, sericite and, in some deposits, sulfate minerals. The stockworks typically vein strongly altered volcanic rocks. This "proximal" alteration typically is dominated by chlorite, sericite, quartz and iron sulfide minerals. In some cases, proximal alteration can contain advanced argillic assemblages (e.g., pyrophyllite, kaolinite) although such zones are much less common than the typical quartz-chlorite-sericite assemblage. Stockwork and proximal alteration zones generally grade outwards over a distance of 10–200 m to lower temperature "distal" alteration zones by either a decrease in alteration intensity or mineralogical changes.

Stockwork zones commonly grade upwards into massive sulfide zones, defined as rock that contains more than 60% sulfide minerals (Sangster and Scott 1976). Although early models interpreted that massive sulfide zones formed at the seafloor (e.g., Hutchinson 1973; Ohmoto 1986; Lydon 1988), more recent work has indicated that massive sulfide zones can also form by replacement of host rocks (Doyle and Allen 2003) or by increasing intensity of stockwork (Fig. 2). Massive sulfide zones are commonly zoned mineralogically and compositionally, typically from Cu-rich at the base to Zn-rich at the top; many Phanerozoic deposits have sulfate-rich zones at the very top. In some cases, massive sulfide zones are flanked by exhalite, chemical sediments formed from hydrothermal fluids that have interacted with seawater. Exhalites can be siliceous and/or iron-rich, can be enriched in many hydrothermal elements, including base metals, and can be deposited hundreds of meters to even kilometers away from massive sulfide deposits (Peter 2003 and references therein). In many, though not all, districts, exhalites mark

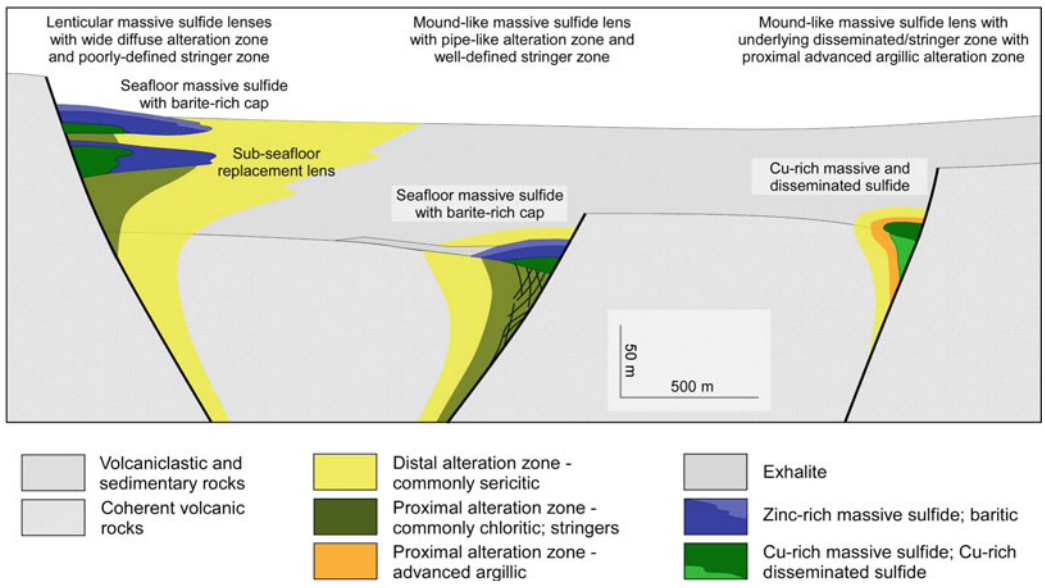

Fig. 2 Idealized cross-section of volcanic-hosted massive sulfide deposits showing different ore and alteration zones

stratigraphic positions prospective for VHMS mineralization.

The right hand inset in Fig. 1 shows a scenario in which the magmatic chamber that drove circulation in the VHMS system also concentrated magmatic-hydrothermal fluids and these were introduced into the circulating VHMS fluid system. In this case both seawater and magmatic volatiles would be fluid sources, and magmatic-hydrothermal sulfur and metals could form a significant component of ore fluid, with the rest derived either from convecting seawater or leaching of the volcanic pile. A mixed fluid with seawater and magmatic-hydrothermal components would then rise to the seafloor, where rapid cooling upon mixing with ambient seawater would cause metal deposition at or just below the seafloor.

3 Stable Isotope Terminology

In this chapter conventional isotopic results are reported relative to internationally recognized standards using standard δ notation: V-SMOW (Vienna-standard mean oceanic water: Werner and Brand 2001) for oxygen and hydrogen and V-CDT (Vienna- Canyon Diablo troillite: Ding et al 2001). Typical 1σ uncertainties in measurements are 0.2‰ for $\delta^{18}O$, 3‰ for δD and 0.2‰ for $\delta^{34}S$. Details of analytical techniques, standards and uncertainties are summarized by Huston et al. (2023).

4 Stable Isotopes and the Genesis of Volcanic-hosted Massive Sulfide Systems

Stable isotope data have played a key role in constraining and understanding fluid and sulfur sources in VHMS mineral systems. Because the oxygen and hydrogen isotope composition of seawater is thought to have been relatively constant over geological time ($\delta^{18}O \sim -3$ to 0‰ and $\delta D \sim -30$ to 0‰: Sheppard 1986), and this value is significantly different to magmatic-hydrothermal fluids ($\delta^{18}O \sim 5.5$ to 10‰ and $\delta D \sim -50$ to −35‰: Taylor 1987), these data can be used to assess the relative importance of evolved seawater and magmatic-hydrothermal fluids in individual VHMS ore systems at the deposit and district scales. Similarly, as the $\delta^{34}S$ composition of seawater sulfate ($\delta^{34}S$ + 10 to + 35‰; Crockford et al. 2019) differs to that of sulfur derived from volcanic or magmatic-hydrothermal sources ($\delta^{34}S$ −5 to + 8‰; Chaussidon et al. 1989), sulfur isotope data have been used to infer the importance of seawater-derived sulfur to the VHMS mineral system through geological time.

4.1 Oxygen and Hydrogen Isotopes

As seawater has oxygen and hydrogen isotope compositions that are significantly different to the rocks that underlie and host VHMS deposits, alteration of these rocks by (evolved) seawater can significantly affect the isotopic composition of the altered rocks. This interaction occurs not only in proximity to the ore zones, but also more regionally. In both cases, oxygen isotope variations have been used to map hydrothermal alteration zones.

4.1.1 Ore-proximal Patterns in Oxygen and Hydrogen Isotopes

Over the last five decades numerous studies (Table E1: updated from Huston 1999) have documented variations in $\delta^{18}O$ and δD in the immediate vicinity of VHMS deposits. These studies have indicated systematic patterns, such as a decrease in $\delta^{18}O$ toward ore (Fig. 3a), that can be used for exploration (e.g., Miller et al. 2001). There are fewer studies documenting variations in δD, and these studies do not show as consistent of a pattern and are likely to be affected by metamorphism. However, despite this, most of the deposits shown in Fig. 3b are characterized by an increase in δD proximal to ore.

Beaty and Taylor (1982) first illustrated these relationships in a diagram schematically illustrating variations in $\delta^{18}O$ away from proximal alteration zones for a range of deposits. Figure 3 is an update of this original diagram that includes many historic studies as well as more recent

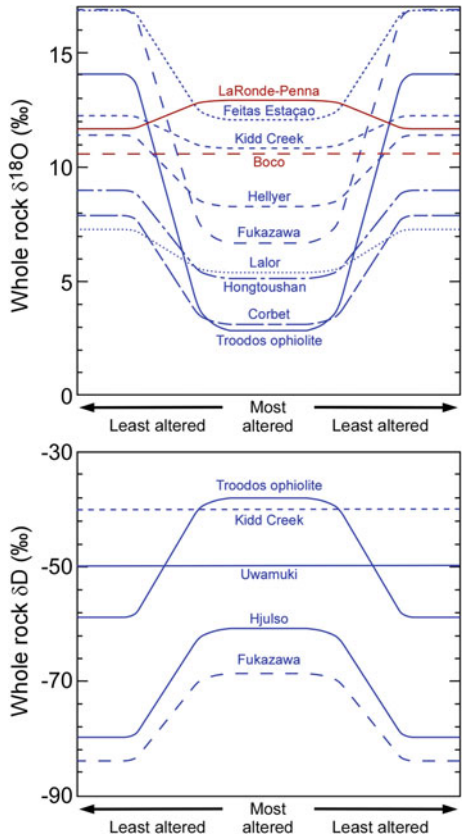

Fig. 3 Schematic diagrams showing variations in whole-rock $\delta^{18}O$ and δD values around VHMS deposits (updated from original diagrams in Beaty and Taylor 1982, using data from Table E1). Because of the large number of studies, this diagram mostly shows deposits with large number of analyses, but also includes some of the classic deposits (e.g., Beaty and Taylor 1982) where the relationship was first demonstrated. The width of the most intense isotopically-altered zone ranges from a few tens to a few hundreds of meters. The scale of the isotopic zonation is up to 1000 m, but more typically a few hundreds of meters

studies that are based on a large number of analyses (most deposits with a small dataset have been excluded, but are summarised in Table E1). At most deposits, there is a consistent pattern of decreasing whole rock $\delta^{18}O$ toward the core of the proximal alteration zone (Fig. 3a). In detail, however, the magnitude and variation between distal and proximal $\delta^{18}O$ varies between deposits and, possibly, through time. Deposits associated with advanced argillic alteration assemblages (red lines in Fig. 3a), however, are characterized by proximal $\delta^{18}O$ values that are similar to or even higher than distal $\delta^{18}O$ values.

To assess possible reasons for this variability, Fig. 4 plots the variation of (a) average distal whole-rock $\delta^{18}O$, (b) average proximal whole-rock $\delta^{18}O$ and (c) the isotopic contrast (i.e. $\delta^{18}O_{distal} - \delta^{18}O_{proximal}$) with geological time. The figure also shows the variations in (d) $\delta^{18}O_{distal}$ versus the isotopic contrast, and (e) $\delta^{18}O_{distal}$ and (f) $\delta^{18}O_{proximal}$ versus 100Cu/(Cu + Zn) of the deposit. No correlation is evident between $\delta^{18}O_{proximal}$ and isotopic contrast, so this diagram is not shown. Although the certainty is limited due to a small sample size, there appears to be a broad decrease in $\delta^{18}O$ values from distal zones and, possibly, proximal zones, with age. Variations in $\delta^{18}O$ in altered rocks are controlled by the temperature of the isotopic exchange, the water/rock (W/R) ratio, $\delta^{18}O$ of the altering fluid and $\delta^{18}O$ and chemical and mineralogical composition of the altered rock.

Figure 4e and 4f indicate that although there is not a relationship between $\delta^{18}O_{distal}$ and 100Cu/(Cu + Zn), low $\delta^{18}O_{proximal}$ alteration zones tend to be associated with Cu-rich deposits. As 100Cu/(Cu + Zn) is a proxy for the overall temperature of the hydrothermal system (e.g., Large 1977; Lydon 1988), this suggests that $\delta^{18}O_{proximal}$ reflects, to a large degree, the overall temperature of the hydrothermal system, particularly in hydrothermal upflow zones with very high W/R. Overall, this temperature has decreased over geological time. The observation that $\delta^{18}O_{distal}$ is unrelated to 100Cu/(Cu + Zn) suggests, however a different control for the isotopic composition of the outer, lower temperature and lower W/R portions of the VHMS mineral system.

A possible reason for the disconnect between $\delta^{18}O_{distal}$ and the overall temperature of the hydrothermal system is that $\delta^{18}O_{distal}$ records a different type of fluid-rock interaction to the high temperature ore fluid. Under conditions of low W/R, the isotopic composition of fluids is largely controlled by the isotopic composition of the rocks with which they interact, in this case the bulk isotopic composition of the rock pile underlying the VHMS deposit. Figure 4a shows that rock pile in which felsic volcanic rocks

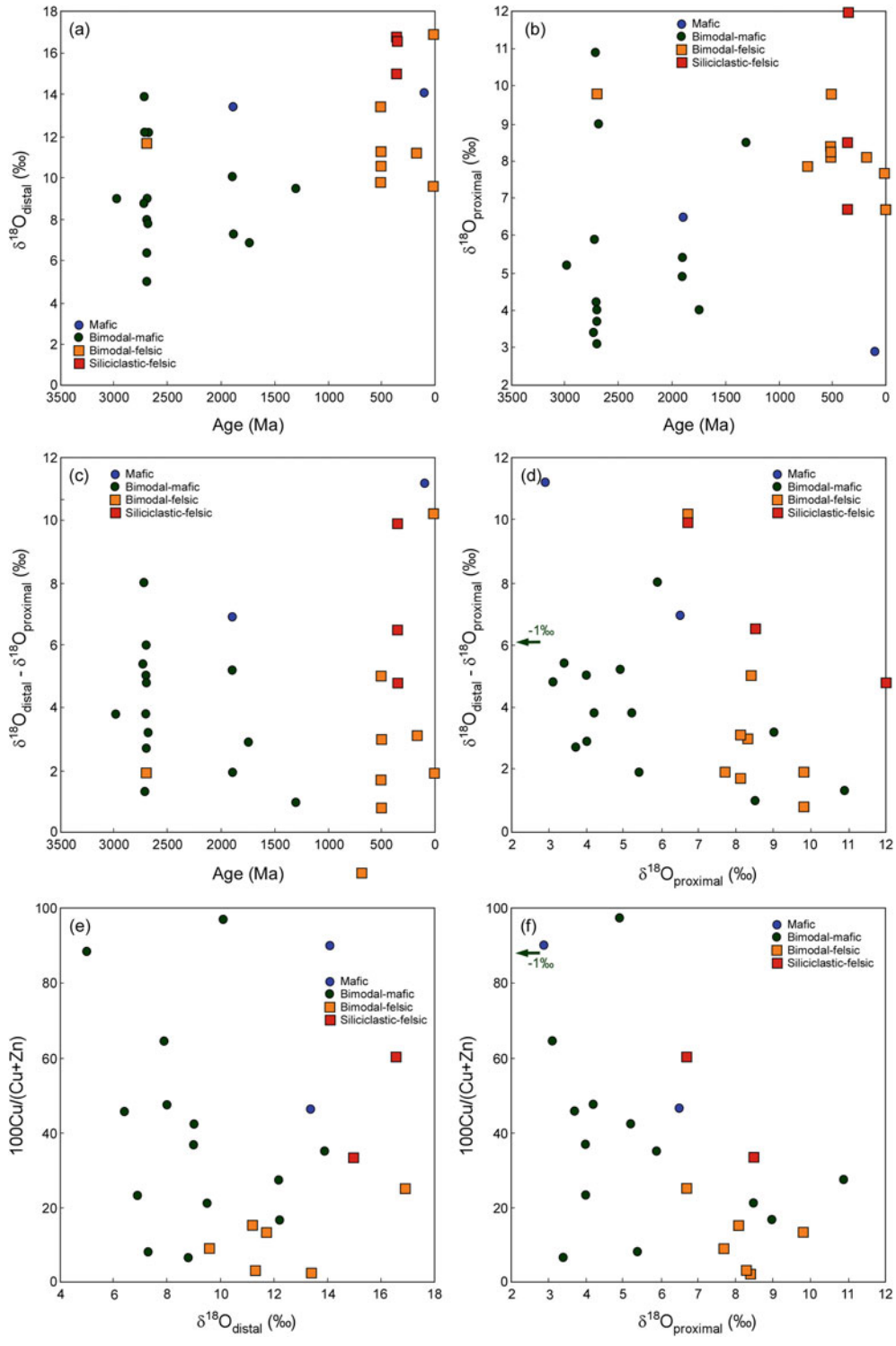

Fig. 4 Plots showing the variation of (a) average distal whole-rock $\delta^{18}O$, (b) average proximal whole-rock $\delta^{18}O$ and (c) the isotopic contrast (i.e. $\delta^{18}O_{distal} - \delta^{18}O_{proximal}$) with geological time, (d) distal $\delta^{18}O$ versus isotopic contrast, and (e) and (f) $\delta^{18}O_{distal}$ and $\delta^{18}O_{proximal}$ versus 100Cu/Cu + Zn) of the associated deposit. Data are from Table E1

dominate have higher $\delta^{18}O_{distal}$ those in which mafic volcanic rocks dominate. As unaltered felsic volcanic rocks (dacite and rhyolite) on average have higher $\delta^{18}O$ (6–9‰) than mafic rocks (basalt: 5–7‰) (Taylor and Sheppard 1986), low temperature, ambient fluids in equilibrium with felsic dominated rock piles under low W/R conditions would have higher $\delta^{18}O$ than fluids equilibrated with mafic-dominated piles. Interaction of such fluids in altered zones distal to the main hydrothermal channelway may account for the observed differences between $\delta^{18}O_{diistal}$ in felsic-dominated and mafic-dominated VHMS systems.

These mechanisms, however, do not directly account for the apparent correlations of $\delta^{18}O_{distal}$ and $\delta^{18}O_{proximal}$ with time (Figs. 4a and 4b); these correlations may be indirect. As shown by Barrie and Hannington (1999) and Huston et al. (2010), deposits in felsic-dominated succession are much more common in the Phanerozoic than in the Paleoproterozoic or Archean; conversely, deposits hosted by mafic-dominated successions are more common in the Paleoprotoerozoic and Archean. Hence, the correlation of $\delta^{18}O_{distal}$ and $\delta^{18}O_{proximal}$ with geological time may relate to the changing relative abundance of mafic- and felsic-dominated volcanic successions as VHMS hosts through time. A possible corollary to this inference is that, on average, older VHMS deposits formed at higher temperatures than younger deposits. Hence, it is important to consider the lithology of the altered host succession when interpreting whole rock $\delta^{18}O$ patterns in the context of genesis and exploration, an issue highlighted by many authors (e.g., Taylor et al. 2015). It also must be stressed that distal values are not those of pristine, unaltered volcanic rocks, but those of rocks that have experienced low temperature, pervasive alteration.

Metamorphic grade also does not seem to affect $\delta^{18}O$ patterns, since regional metamorphism most commonly did not involve significant water advection, and is considered isochemical (Riverin and Hodgson 1980); thus, variations in $\delta^{18}O$ see through regional metamorphism and reflect original fluid-rock interaction patterns and pathways.

As discussed below the difference in the isotopic patterns associated with deposits associated with advanced argillic alteration zones to those deposits associated with the typical chlorite and/or sericite dominated alteration assemblages could be caused by interaction of lower temperature hydrothermal fluids or by ore fluids with higher $\delta^{18}O$, such as magmatic-hydrothermal fluids (e.g., Beaudoin et al. 2014). In high sulfidation epithermal deposits, which are typically associated with advanced argillic alteration assemblages, the advanced argillic assemblages are typically interpreted to be the consequence of acidic fluids formed by the dissociation of SO_2 at high temperature (> 350 °C) in magmatic-hydrothermal fluids (Ohmoto and Rye 1979; Rye et al. 1992). Similar processes are envisioned to have occurred in VHMS deposits that have been influenced by magmatic-hydrothermal fluids, leading to hydrothermally altered rocks with elevated $\delta^{18}O$ (e.g., Sillitoe et al. 1996; Huston et al. 2011).

In general, oxygen and, to a lesser extent, hydrogen isotopes are zoned about VHMS deposits due to hydrothermal alteration associated with the ore-forming fluids. In detail, however, the patterns can be complicated and can be affected by the protolith lithological variability of the altered rocks. To illustrate this we summarize the results of some of the more detailed oxygen and hydrogen isotope studies to illustrate the similarities, and differences, in the isotopic patterns.

Hokuroku district, Japan. In the Miocene Hokuroku district of Japan, Hattori and Muehlenbachs (1980), Green et al. (1983) and Urabe et al. (1983) documented variations around bimodal felsic VHMS deposits of this district. Of the deposits described, the most information is available from the Fukazawa deposit (Green et al. 1983: Fig. 5a). Green et al. (1983) documented a zone with $\delta^{18}O$ below 8‰, which corresponds almost directly to the sericite-chlorite alteration zone that cuts stratigraphy and forms a pipe that extends below and above the orebody. This zone is surrounded by a 500–1500-m-wide, montmorillonite-altered halo that is characterized by $\delta^{18}O$ values between 8‰ and

14‰. Lateral to the montmorillonite zone, the rocks have been quartz- and zeolite-altered with $\delta^{18}O$ values above 14‰ (Date et al. 1983; Green et al. 1983).

Noranda district, Québec, Canada. Beaty and Taylor (1982) documented variations in whole rock $\delta^{18}O$ data along a traverse across the alteration pipe (in a similar position to stockwork zones in other VHMS deposits) at the Amulet deposit in the Noranda district, Québec (Fig. 5b), showing a pattern about the alteration pipe, with the central, most intensely, chlorite-altered part

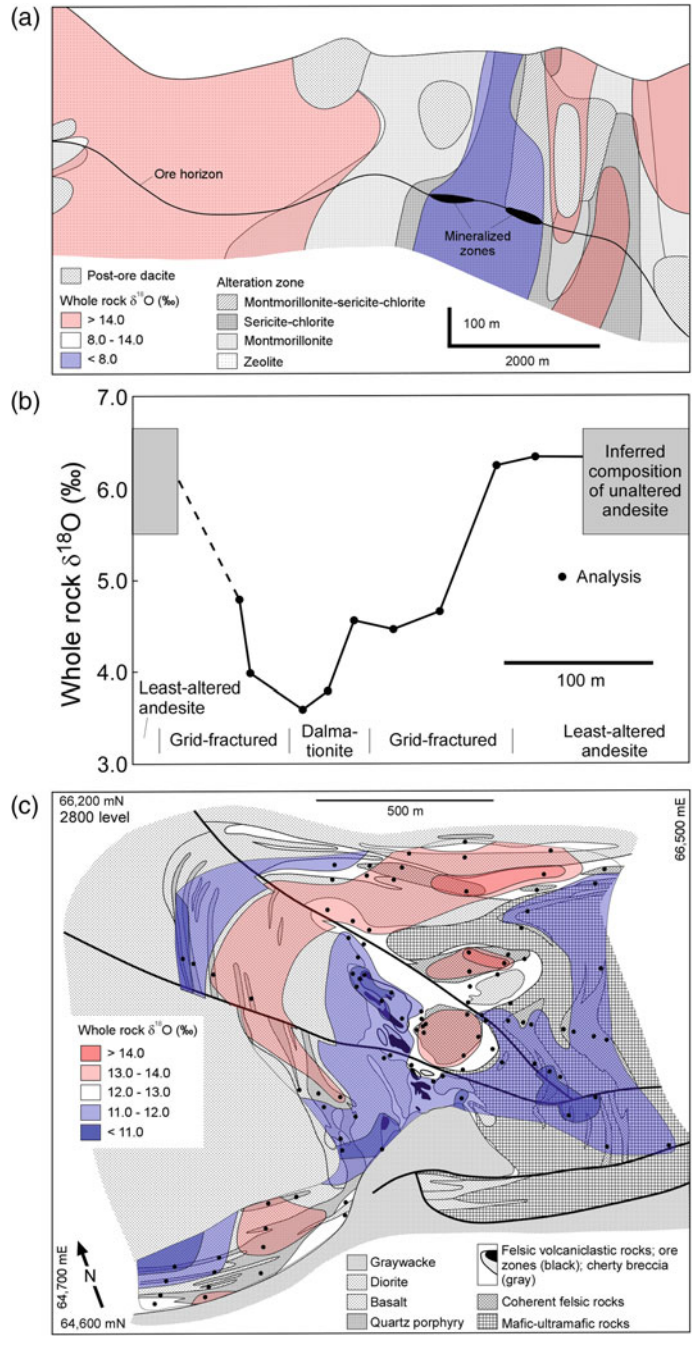

Fig. 5 Sections and plans showing proximal whole-rock $\delta^{18}O$ variations around VHMS deposits: (a) Fukazawa deposit, Hokuroku district, Japan (modified after Green et al. 1983), (b) Amulet deposit, Quebec, Canada (modified after Beaty and Taylor 1983) and (c) Kidd Creek deposit, Ontario, Canada (modified after Huston and Taylor 1999). "Dalmationite" in (b) refers to a metamorphosed, intensely altered zone consisting of coarse-grained cordierite porphyroblasts set in a fine-grained chlorite-quartz-anthophyllite matrix. "Grid-fractured" refers to a biotite-rich rock with a grid-like network of quartz-filled fractures

of the pipe having a $\delta^{18}O$ values of 3.6–4.0‰ that increased over a distance of 150 m outward to 6.0–6.7‰ in least altered volcanic rocks. Beaty and Taylor (1982) also demonstrated that, with the exception of the Kidd Creek deposit (see below), this pattern was consistent through most deposits that had been studied at that time.

In the New Vauze-Norbec area in the central part of the Noranda volcanic complex, Paradis et al. (1993) showed an up stratigraphy increase in $\delta^{18}O$, from values near 2‰ at the bottom of the stratigraphic section, to values near 14‰ at the top. This stratigraphic variation was interpreted to have formed under an increasing thermal gradient and increasing water/rock exchange during the cooling of the Flavrian syn-volcanic intrusion. Paradis et al. (1993) proposed that the hydrothermal fluid was Archean seawater with $\delta^{18}O$ near 0‰ that evolved through water–rock isotope exchange to a heavier composition.

The variations in $\delta^{18}O$ described above are one-dimensional transects or drill holes or two dimensional plans or sections. Taylor et al. (2014) determined three-dimensional variations in whole rock $\delta^{18}O$ at the Horne and Quemont deposits within the Noranda district, which combined have produced over 10 Moz of gold. The surface expression of the Horne deposit is associated with a zone of low $\delta^{18}O$ (< 6‰), as seen in other deposits discussed above. Zones of high (> 9‰) $\delta^{18}O$ distal to the deposits may indicate low temperature alteration peripheral to the higher temperature alteration. These data, data from elsewhere in the Noranda district (see below) and from Kidd Creek indicate that persistent zones of relatively high $\delta^{18}O$ may indicate the lack of significant high temperature fluid flow and downgrade exploration potential of these zones, although it must be stated that deposits associated with advanced argillic alteration zones may not be associated with proximal $\delta^{18}O$ depletion zones.

Kidd Creek deposit, Ontario, Canada. The ~ 2714 Ma Kidd Creek deposit (147.88 Mt grading 2.31% Cu, 6.18% Zn, 0.22% Pb, 87 g/t Ag and 0.01 g/t Au) is the only significant deposit in the Kidd-Munro assemblage in eastern Ontario, Canada. It consists of several steeply-plunging orebodies that are hosted by a mainly rhyolitic volcaniclastic unit within a succession dominated by mafic volcanic rocks (Huston and Taylor 1999: Fig. 5c). The orebodies occur along the southeastern limb of a tight, steeply-plunging anticline.

The first oxygen isotope study by Beaty et al. (1988) at Kidd Creek demonstrated that $\delta^{18}O$ values in proximal quartz-rich alteration assemblages, at 10–12‰, were much higher than the $\delta^{18}O$ values of other VHMS deposits, and that these values increased stratigraphically below the ore zone to values of 13–16‰ in felsic rocks. Beaty et al. (1988) interpreted these results as indicative of a two-stage hydrothermal system, with the main stage fluids having values of 6–9‰.

Huston and Taylor (1999) followed these initial studies with a more detailed study. They found that the $\delta^{18}O$ values are influenced by the original lithology of altered rocks; Fig. 4c shows variations in $\delta^{18}O$ only of samples with rhyolitic protoliths as determined by lithological observations (e.g., the presences of quartz phenocrysts) or the geochemistry of immobile elements. The lowest $\delta^{18}O$ values (<11‰) at Kidd Creek are associated with the "cherty breccia" alteration facies that is closely associated with the ore lenses, a result consistent with Beaty et al. (1988). Huston and Taylor (1999) also found that $\delta^{18}O$ values increase both laterally away from and stratigraphically above the ore zones to values that exceed 14‰. The host succession includes both fragmental and coherent rhyolitic rocks. Coherent units stratigraphically below or at the same position as the ore lenses are characterised by high δO values (> 13‰) that are interpreted to be the consequence of low temperature alteration that silicified these units. These rocks then became impermeable to later, higher temperature fluid flow, preserving the ^{18}O-enriched signature and focussing fluid flow into fragmental rocks. These fragmental rocks were strongly affected by these later high-temperature fluids, which produced the cherty breccia and the ^{18}O-depleted zone associated with the ore lenses (Fig. 5c: Huston and Taylor 1999). This may have produced the isotopic

disequilibria that Beaty et al. (1988) interpreted to indicate two hydrothermal stages.

Stratigraphically above the ore position, $\delta^{18}O$ data define an ^{18}O-enriched ($\delta^{18}O > 13‰$) zone that forms a carapace that has been folded by the later anticline. This zone is interpreted to have formed as the result of lower temperature alteration associated with the cooling of the Kidd Creek hydrothermal system. This carapace is only breached above the southwest ore lens (Huston and Taylor 1999), and may indicate limited high-temperature fluid flow after the Kidd Creek deposit was covered by later volcanic rocks. $\delta^{18}O$ patterns around the Kidd Creek deposit not only provide vectors toward ore, but they also provide constraints on ore fluid hydrology before, during and after ore formation.

LaRonde deposit, Québec, Canada. The LaRonde deposit (58.76 Mt grading 0.33% Cu, 2.17% Z, 45 g/t Ag and 4.31 g/t Au) is hosted by dacitic to rhyolitic rocks of the Bousquet Formation, Blake River Group (2699–2697 Ma, Mercier-Langevin et al. 2007). The deposit consists of four stacked semi- to massive sulfide lenses within complexly zoned alteration assemblages that has been metamorphosed at lower amphibolite facies to assemblages of mostly quartz, biotite, chlorite, garnet, muscovite, staurolite, rutile and pyrite. An unusual characteristic of the deposit is the presence of an aluminous alteration zone consisting of quartz, kyanite, andalusite, muscovite and pyrite (Dubé et al. 2007). $\delta^{18}O$ values of the altered host rocks range between 9.0 and 14.2 ‰ for all but 2 analyses, with average $\delta^{18}O$ values of different alteration facies between 9.8 and 12.9‰ and the aluminous facies having the highest $\delta^{18}O$ (Beaudoin et al. 2014).

Fluid-rock modelling indicates that the high $\delta^{18}O$ values at LaRonde can be explained by reaction of volcanic rocks with an initial $\delta^{18}O$ value of 7–9‰ with a fluid with initial $\delta^{18}O$ close to 5‰, at temperatures of 100–200ºC, under W/R ratios up to 50:1 (Beaudoin et al. 2014). These W/R ratios are typical of proximal alteration zones, which are fluid dominated, as shown by Green et al. (1983), Shanks (2014) and many others. As these proximal alteration zones define fluid conduits, they have much higher W/R ratios than the VHMS system as a whole.

The initial fluid composition of 5‰ was interpreted to have been evolved seawater perhaps mixed with a magmatic water component exsolved from dacitic to rhyolitic magma, consistent with the aluminous alteration interpreted to be metamorphosed advanced argillic alteration analogous to subaerial high-sulfidation epithermal environments (Dubé et al. 2007).

4.1.2 District-scale Patterns in Oxygen Isotopes

Although most $\delta^{18}O$ patterns have been established in the immediate vicinity of VHMS deposits, there are several more regional studies, including studies of the ~ 400 Ma West Shasta district in California, USA (Taylor and South 1985), the ~ 2698 Ma Noranda district in Quebec, Canada (Cathles 1993), the ~ 2714 Ma Kidd-Munro district in Ontario, Canada (Taylor and Huston 1999), the ~ 3240 Ma Panorama district in Western Australia (Brauhart et al. 2000), the ~ 2745 Ma Sturgeon Lake district in Ontario, Canada (Holk et al. 2008) and the ~ 2681 Ma Izok Lake district in Nunavut, Canada (Taylor et al. 2015). Of these the two best documented districts, Noranda and Panorama, are described below.

Noranda, Québec, Canada. The Noranda district in the Superior Province, Québec, is a classical VHMS district that rests undeformed since its formation (~2700 Ma), with only a shallow tilt to the east. The district is hosted by a sequence of bimodal mafic-felsic volcanic rocks of the Blake River Group. The Noranda Volcanic Complex hosts 18 VHMS deposits that have yielded 48.5 Mt of ore, in addition to the Horne deposit (54.3 Mt) and its undeveloped Horne 5 zone (~150 Mt; Kerr and Gibson 1993). A seminal study by Cathles (1993) documented the plan view of the VHMS system from 588 oxygen isotope analyses (Fig. 6) and was augmented by 599 analyses by Taylor and Timbal (2002). These studies show that the syn-volcanic Flavrian pluton is surrounded by an annular zone with $\delta^{18}O$ values < 6‰ that extend up section as six fingers that point toward most of the VHMS

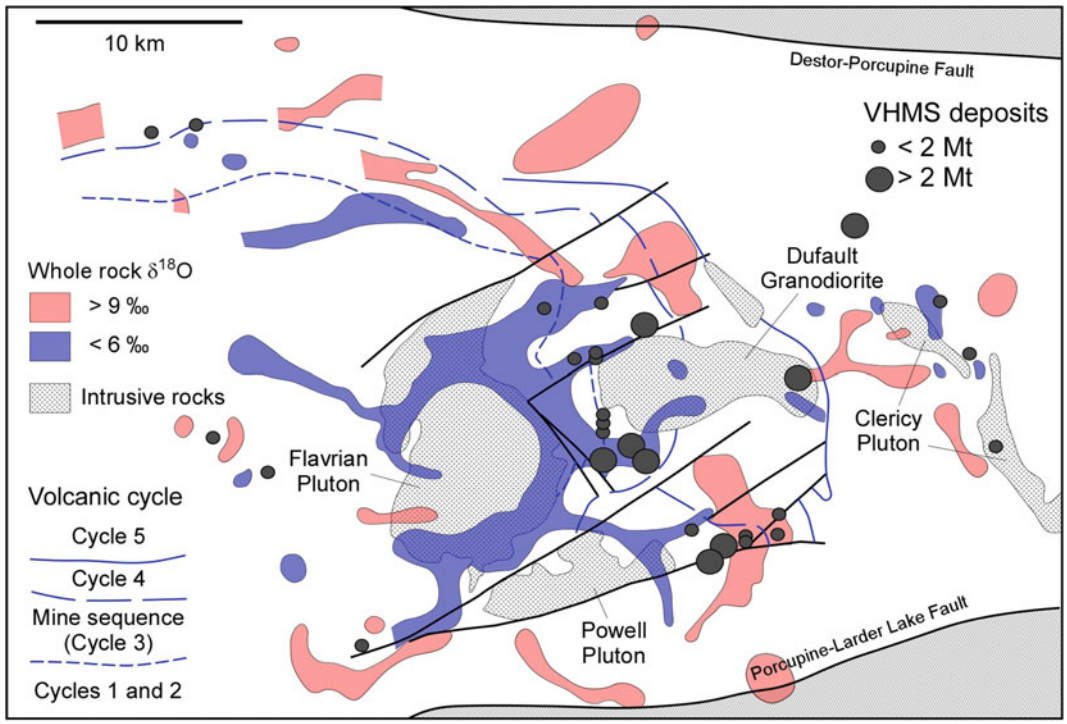

Fig. 6 Whole-rock $\delta^{18}O$ variations in the Noranda district, Quebec, Canada (modified after Cathles 1993, to incorporate geological data from Kerr and Gibson 1993)

deposits of the district (Fig. 6: Cathles 1993). Stratigraphically above the low $\delta^{18}O$ fingers and most VHMS deposits, the volcanic rocks have $\delta^{18}O$ values > 9‰, interpreted to represent the reaction of the volcanic rocks above the deposits with cooled hydrothermal fluids, thus forming a cap rock indicative of underlying higher temperature hydrothermal fluid activity (Cathles 1993; Taylor and Holk 2002).

Panorama, Western Australia. The ~ 3238 Ma (Buick et al. 2002) Panorama district in the East Pilbara Terrane of Western Australia is the oldest significant VHMS district known, and also one of the best preserved. The district contains two economically significant deposits including Sulphur Springs (13.8 Mt grading 3.8% Zn, 0.2% Pb, 1.5% Cu and 17.0 g/t Au) and Kangaroo Caves (3.8 Mt grading 6.0% Zn, 0.3% Pb, 0.8% Cu and 15.0 g/t Au) among several smaller deposits and prospects hosted at or near the top of the bimodal volcanic Kangaroo Caves Formation. Although the district has seen only sub-greenschist metamorphism, the host succession has been structurally tipped on its side, providing an oblique cross-section of the underlying sub-volcanic Strelley Granite, through the host Kangaroo Caves Formation, and into the overlying turbidites of the Soanesville Group (Fig. 7a). This volcanic succession was extensively altered, with systematic zonation in alteration assemblages at the district scale. Brauhart et al. (1998) found that the lower part of the volcanic succession is dominated by a semi-conformable chlorite-quartz alteration zone that becomes transgressive, forming cross-cutting pipes below major deposits such as Sulphur Springs and Kangaroo Caves. This chlorite-rich zone grades upward from the semi-conformable zone and outward from the cross-cutting pipes into semi-conformable sericite-quartz and feldspar-sericite-quartz zones.

As part of a district-scale alteration study, Brauhart et al. (2000) analyzed 188 volcanic and granite samples for both oxygen isotopes and whole rock geochemistry. Figure 7b shows the

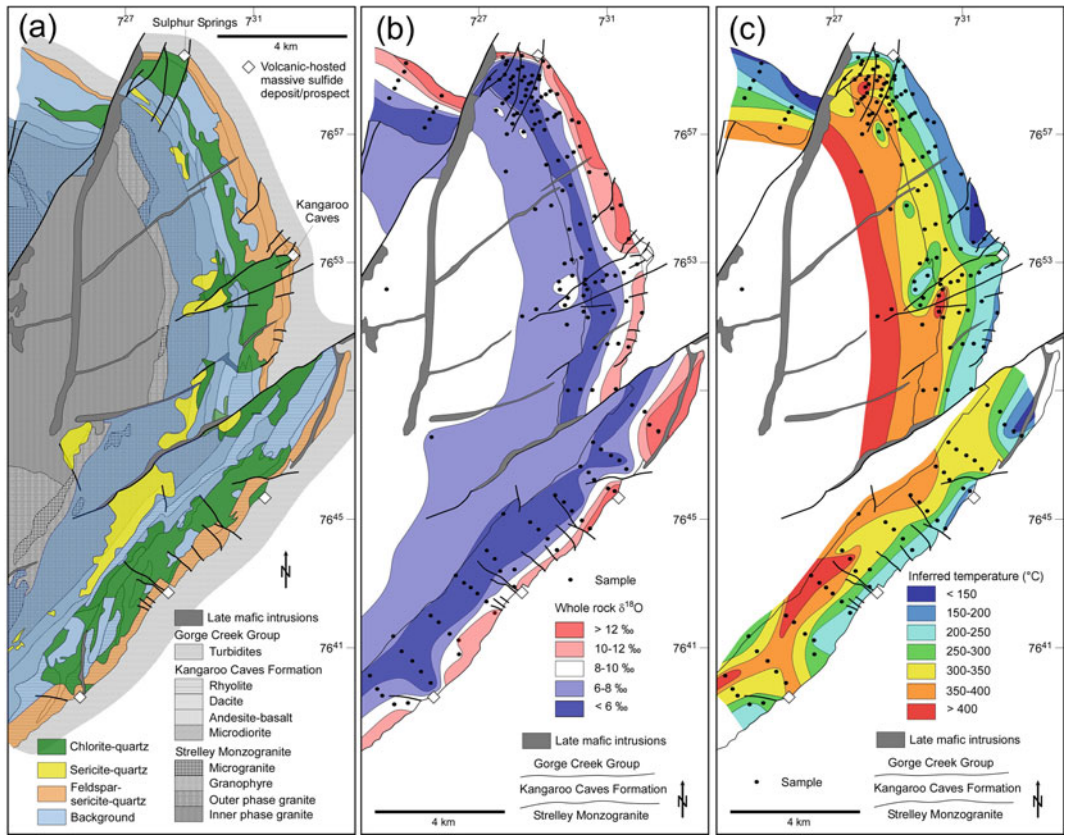

Fig. 7 Maps of the Panorama VHMS district showing (a) geology and alteration zonation, (b) whole-rock $\delta^{18}O$ variations, and (c) variations in estimated hydrothermal temperatures calculated from whole-rock $\delta^{18}O$ and geochemical data (modified after Brauhart et al. 2000). The "background" alteration assemblage refers to spilitic assemblages in basalt or keratophyric assemblges in felsic rocks and typified by the presence albite-, K-feldspar-chlorite- and/or ankerite-quartz-pyrite-dominant assemblages (Brauhart et al. 1998)

distribution of $\delta^{18}O_{whole\ rock}$ from these data. The zone with the lowest $\delta^{18}O$ (< 6‰) corresponds closely with the semi-conformable chlorite-quartz alteration zone in the lower part of the volcanic pile. $\delta^{18}O$ increases upwards through the volcanic pile to values of 12–14‰ at the top. The higher $\delta^{18}O$ values correspond to the sericite-quartz and feldspar-sericite-quartz alteration zones. Like the chlorite-quartz alteration zones, pipes of low $\delta^{18}O$ values extend from the basal zone below the locations of known VHMS deposits. The pipe that extends below Sulphur Springs has $\delta^{18}O$ values of < 6‰, whereas the pipe that extends below Kangaroo Caves has values of 6–8‰. This observation is consistent with deposit-scale patterns in which Cu-rich deposits are associated with stronger $\delta^{18}O$ anomalies than Zn-rich deposits.

Following the method of Miller et al. (2001) and using mineral abundances calculated from the whole rock geochemical data, Brauhart et al. (2000) estimated the fractionation function between the altered rock and altering fluid ($\Delta^{18}O_{whole\ rock\text{-}fluid}$). They then calculated the temperature of alteration using the $\Delta^{18}O_{whole\ rock\text{-}fluid}$ functions and assuming $\delta^{18}O_{fluid}$ (Fig. 7c). Using a $\delta^{18}O_{fluid}$ of 2‰ suggested that alteration temperatures locally exceeded 400 °C in the high temperature, semi-conformable chlorite-rich part of the alteration system, within and just above the Strelley Granite. The alteration temperature decreased, in general, upward to the contact with

the overlying Soanesville Group, where the temperature was generally below 200 °C. Immediately below the Sulphur Springs and Kangaroo deposits, the chlorite-rich alteration zones become transgressive, connecting the semi-conformable zone at the base of the volcanic pile with individual deposits. The $\delta^{18}O_{\text{whole rock}}$ and calculated temperature also reflect this alteration pattern, with these data also defining transgressive zones connecting the high temperature semi-conformable alteration zone with the proximal alteration zones associated with the deposits. Although a $\delta^{18}O_{\text{fluid}}$ value of 2‰ was assumed in Fig. 6c, changing this assumed value does not change the relative temperature patterns even though the absolute temperatures estimated do change.

4.1.3 Implications of δ^{18}O-δD Data to Determining Fluid Sources

Oxygen and hydrogen isotope data were a key piece of evidence that was used to argue that ore fluids that formed VHMS deposits were evolved seawater (Ohmoto et al. 1983). Since then, the gathering of new data has indicated a more complicated picture, although evolved seawater still appears to be the most important ore fluid. Table 1 (updated from Huston 1999; this table excludes deposits metamorphosed at grades of amphibolite or higher and some deposits (e.g., Raul, Peru) for which a VHMS origin has been questioned) and Fig. 8 summarize the $\delta^{18}O$ and δD characteristics of VHMS ore fluids as deduced from deposits that have not undergone high-grade metamorphism (amphibolite or greater) that may disturb the original isotopic characteristics.

Most VHMS deposits have fluid δ^{18}O-δD signatures similar to seawater. In general, $\delta^{18}O$ values are within 2‰ and δD values are within 20‰ of standard mean oceanic water (SMOW). These values are consistent with evolved seawater being the dominant ore fluid (Fig. 8b).

As discussed above, currently active seafloor systems provide information, such as direct measurements of the isotopic composition of mineralizing fluids and the isotopic response (and geochemical response in general) of these

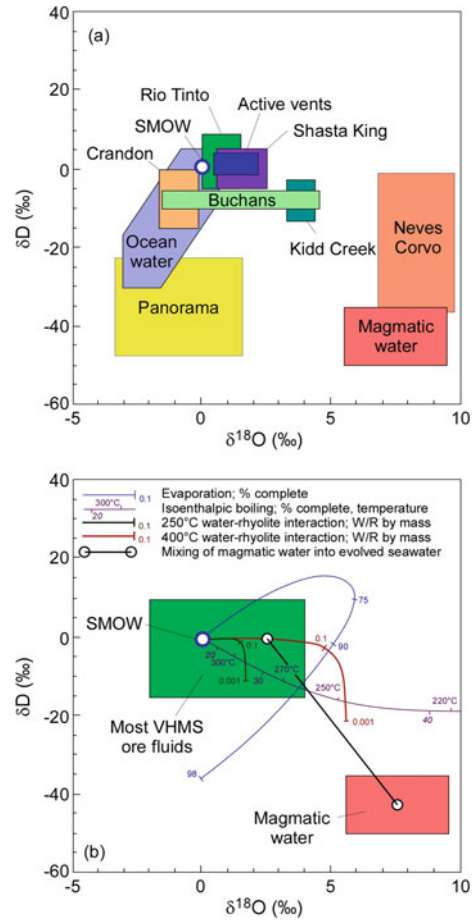

Fig. 8 δ^{18}O-δD diagrams showing (a) the fields of selected VHMS ore-forming fluids (from Table 1) and the fields of seawater and magmatic water (Sheppard, 1986; Taylor, 1992), and (b) paths showing the evolution of seawater undergoing evaporation (Knauth and Beeunus, 1986), open-system water–rock interaction (e.g., Taylor 1987), adiabatic boiling (using data of Friedman and O'Neil (1977) and Keenan et al. (1969)), and mixing with magmatic water (updated from Huston 1999)

fluids to geological perturbations of the mineral system. Although much of the data come from active deposits not associated with convergent margins, the data provide general guidance for seafloor mineral systems. The vent fluids tend to have $\delta^{18}O$ 0.5–1.0‰ heavier than, and δD values very similar to ambient seawater (Shanks 2001), which supports the inference (e.g., Ohmoto et al. 1983) that evolved seawater was the dominant fluid source in most VHMS mineral systems.

There are, however, several important exceptions to the inference that seawater is the dominant fluid source, including several deposits in the ca 350 Ma Iberian Pyrite Belt, and the ca 2698 Ma Horne, ca 2714 Ma Kidd Creek and ca 2736 Ma South Bay deposits of the Superior Province, Canada. These data may indicate a significant contribution of other fluid sources, particularly magmatic-hydrothermal fluids, in a limited number of deposits (Fig. 8b).

The best case for a significant magmatic-hydrothermal component is the Neves Corvo deposit in the Iberian Pyrite Belt, which has the highest estimated $\delta^{18}O_{fluid}$ from a VHMS deposit at 8.3 ± 1.5‰ (Relvas et al. 2006). This deposit is a highly unusual for VHMS deposits in being very Sn-rich, with abundant pyrrhotite, not unlike some carbonate-replacement tin deposits that are typically thought to be magmatic-hydrothermal in origin (e.g., Blevin and Chappell 1995). Some of the other deposits with high $\delta^{18}O_{fluid}$ are associated with advanced argillic alteration assemblages, for example the Boco deposit in Tasmania (Herrmann et al. 2009), an alteration assemblage possibly indicative of a magmatic-hydrothermal contribution (Huston et al. 2011). The unusually ^{18}O-enriched signature of advanced argillic assemblages at the LaRonde-Penna district could also be the product of magmatic-hydrothermal contribution (see above and Beaudoin et al. 2014). Hence it would appear that there is a significant subclass of VHMS deposits in which a significant magmatic-hydrothermal contribution is likely, but for most of these deposits the most likely fluid source is evolved seawater. A small contribution of magmatic-hydrothermal fluids, however, would be diluted by the dominant evolved seawater contribution and not visible in stable isotopic data. Such a contribution may be visible in other data, for example metal budgets, and remains an important line of enquiry for future research on VHMS deposits.

In other districts, however, seawater-dominated hydrothermal systems, which form VHMS deposits, are physically separated from coeval hydrothermal systems developed in subvolcanic intrusions. Drieberg et al. (2013) showed this in the Panorama district. The ore fluids that formed the VHMS deposits had lower salinity, density and $\delta^{18}O_{fluid}$ (Table 1) than fluids that formed Sn-Cu–Zn and Mo mineral occurrences near the upper margin of the granite. Drieberg et al. (2013) concluded that density differences and low permeability barriers prevented the mixing of the seawater-dominated hydrothermal system in the volcanic pile with the magmatic-hydrothermal system in the granite.

4.1.4 Application of Oxygen and Hydrogen Isotope Geochemistry to Exploration and Ore Genesis

Data from well-studied deposits described above, combined with additional data presented in Table E1, indicate that oxygen isotope data define high-temperature fluid pathways associated with VHMS deposits at the deposit scale. For most deposits, high temperature alteration zones are associated with ^{18}O depletion anomalies (low $\delta^{18}O$) that can extend up to several hundreds of meters laterally from ore and greater distances with depth. In some cases the low $\delta^{18}O$ anomalies also extend above the deposit to define a hanging wall alteration zone.

The data also indicate changes in isotopic patterns with geological time and deposit type. $\delta^{18}O$ values of proximal alteration zones are higher for deposits in felsic-dominated succession than those hosted by mafic-dominated successions. This may simply reflect the temperature of upflow, which, based on 100Cu/(Cu + Zn) is likely to be higher in the mafic-dominated systems. The variation in time may relate to the greater abundance of felsic-dominated, lower temperature systems at younger times in Earth's history.

The main exceptions to the general patterns described above are deposits in which a significant magmatic-hydrothermal component in inferred (see also below). In these cases (Kidd Creek, LaRonde and Boco: Table 1), the ^{18}O depletion anomaly is suppressed or can present as a weak ^{18}O enrichment anomaly (Fig. 3). Hence, it is important to interpret oxygen isotope

data in a geological context including the age, host succession and type of deposit being targeted.

Studies of the Noranda and Panorama districts demonstrate that district-scale variations in whole-rock $\delta^{18}O$ data correlate to variations in alteration assemblages and provide district-scale vectors to ore. The variations most likely relate to temperature gradients within the hydrothermal system. Other studies, including those at West Shasta (Taylor and South 1985), Izok Lake (Taylor et al. 2014), Kidd-Munro (Taylor and Huston 1999), and Sturgeon Lake (Holk et al. 2008) districts, demonstrate broadly similar relationships. The relative intensity of the anomaly at the district scale may also be indicative of the Cu:Zn ratio of associated deposits as it is at the deposit scale.

In many cases low-$\delta^{18}O$, high temperature alteration zones associated deposits are surrounded or capped by zones of higher $\delta^{18}O$. These zones, which are not readily identified by mineralogical or geochemical alteration mapping, represent lower temperature alteration zones, and regional gradients from these zones toward higher-temperature zones can be used as district-scale vectors.

Overall, whole rock oxygen isotopes allow detection of the infiltration of hydrothermal fluids, and mapping of the fluid pathways, which enable targeting for VHMS mineralization. Several characteristics of VHMS systems can be uniquely recognized using stable isotopes: (1) a syn-volcanic intrusion driving hydrothermal fluid flow during cooling will be overlain by a high-temperature alteration with low $\delta^{18}O$ values, providing a regional exploration target for a potentially fertile syn-volcanic intrusion; (2) discordant zones of low $\delta^{18}O$ values map the zones of hydrothermal fluids flow up-section on top of which VHMS deposits are most likely located; (3) discordant to semi-concordant zones of high $\delta^{18}O$ values record the waning upflow of hydrothermal fluids at lower temperatures, which sits above of the higher temperature up-flow zone in the underlying stratigraphic section of volcanic rocks, and thus enabling targeting of blind high temperature (low $\delta^{18}O$) up-flow zones.

4.2 Sulfur Isotopes

Sulfur is an important component of the VHMS mineral system for two reasons. First, as iron and base metal sulfides are very insoluble at low to moderate temperatures, the presence of H_2S precipitates iron and base metal sulfides when high temperature, H_2S-rich ore fluids quench as they reach the seafloor. Second, some metals, for instance gold, are transported by sulfide complexes. In reduced hydrothermal upper crustal fluids, sulfur (as H_2S) can be sourced from sulfide leached from the underlying volcanosedimentary succession, thermochemical sulfate reduction of seawater (TSR), either at depth or in the near-surface during fluid upflow, and/or disproportionation of magmatic SO_2 (c.f. Ohmoto 1996). The sulfur isotope composition of sulfides in all mineral systems reflects not only the sulfur source but geochemical interactions between magmas, fluids, host rocks, and seawater, that lead to precipitation of sulfide minerals (Ono et al. 2007; Peters et al. 2010; LaFlamme et al. 2018; Martin et al. 2021; Huston et al. 2023). Owing to the high temperature of the upflow zones of VHMS deposits (Eldridge et al. 1983; Ohmoto 1986), it is unlikely that bacterial sulfate reduction (BSR) played a role in an important role in the core of VHMS systems, although in some deposits BSR may have been an important processes in the lower temperature peripheries to VHMS systems (see below).

4.2.1 Secular Variations in Sulfur Isotope Ratios from Volcanic-hosted Massive Sulfide Deposits

Figure 9 illustrates changes in $\delta^{34}S$ of sphalerite and sulfate minerals from VHMS deposits with geological time based upon a compilation of data by Huston et al. (2022: Table E2). Sphalerite was used for this analysis as it forms almost entirely as the result of hydrothermal activity and therefore records the characteristics of hydrothermal sulfur. Although it would be ideal to also consider $\delta^{34}S$ variations of chalcopyrite with geological time, as it reflects higher temperature parts of the VHMS system, an analogous

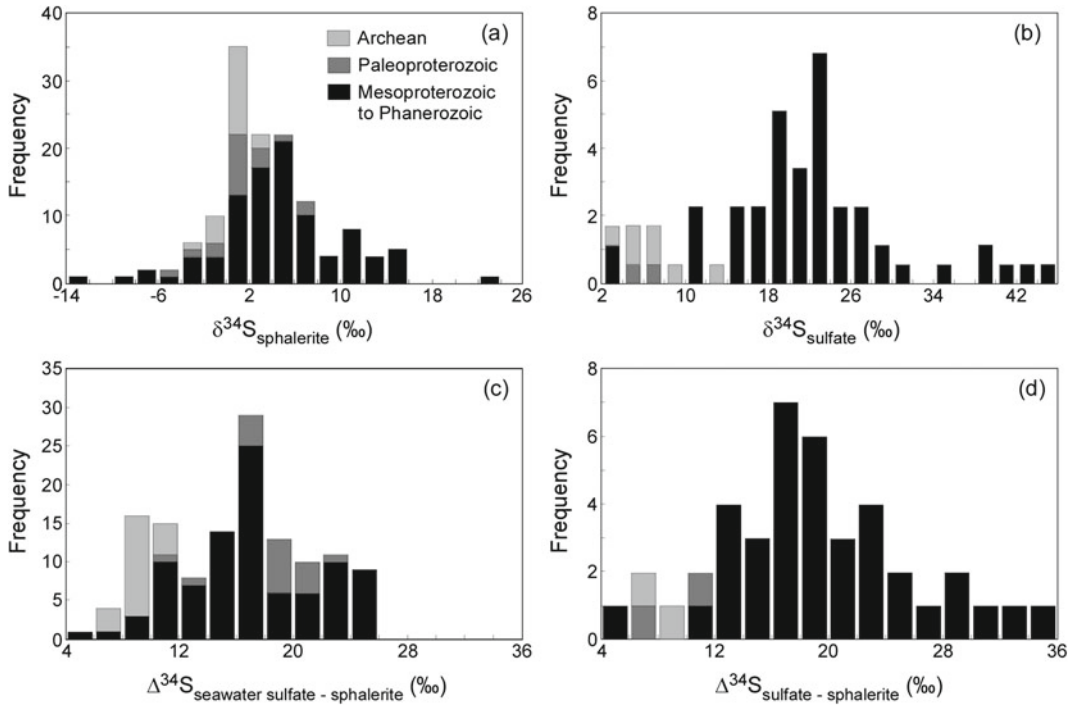

Fig. 9 Histograms showing (a) variations in median $\delta^{34}S$ values of sphalerite, (b) variations in median $\delta^{34}S$ values of sulfate minerals, (c) $\Delta^{34}S_{\text{seawater sulfate-sphalerite}}$ (estimated from secular seawater sulfate variations and median sphalerite values), and (d) $\Delta^{34}S_{\text{sulfate-sphalerite}}$ (using median sulfate and sphalerite values for individual deposits). Median mineral $\delta^{34}S$ data are from Huston et al. (2022), and seawater sulfate data are after Crockford et al. (2019) supplemented by Neo- and Paleoarchean barite data summarised in Huston et al. (2022)

compilation of chalcopyrite does not exist. As minerals such as pyrite and pyrrhotite do not form exclusively from hydrothermal processes they can reflect the input of non-hydrothermal sulfur produced by biological and other processes.

Although limited by the concentration of deposits into restricted time intervals, there are some relatively consistent patterns in the data. The most prominent pattern is the relatively consistent values of median $\delta^{34}S_{\text{sphalerite}}$ of Paleoproterozoic (-4.6‰ to 6.5‰, median = 1.7‰, n = 18: Fig. 9a) and Archean (-2.8‰ to 2.4‰, median = 0.8‰, n = 20) deposits at around 0‰. This contrasts with the much greater variability of deposits of Mesoproterozoic-Phanerozoic age (-13.7‰ to 23.9‰, median = 4.6, n = 96). $\delta^{34}S_{\text{sulfate}}$ shows a similar pattern, although shifted to higher values (Fig. 8b). For Mesoproterozoic-Phanerozoic deposits, the range is 3.5‰ to 44.4‰ with a median of 22.2‰ (n = 56), for Paleoproterozoic deposits the range is 4.4‰ to 11.0‰ with a median of 8.8‰ (n = 4), and for Archean deposits the range is 3.8‰ to 13.2‰ with a median of 6.2‰ (n = 7).

Sangster (1968) was the first to document the variability in $\delta^{34}S$ data in Phanerozoic VHMS and sediment-hosted deposits. He found that $\delta^{34}S_{\text{sulfate}}$ in these deposits was similar to the $\delta^{34}S_{\text{sulfate}}$ of coeval seawater. The right-hand side of Fig. 10 illustrates this relationship. Sangster (1968) also noted that $\delta^{34}S_{\text{sulfide}}$ values are 17.5 ± 2.5‰ (1σ) lower than coeval seawater, a relationship that has held up even as the sulfur isotope database has increased (Fig. 9c; see also Huston 1999). The similarity between VHMS $\delta^{34}S_{\text{sulfate}}$ and coeval seawater $\delta^{34}S_{\text{sulfate}}$ is most simply interpreted to indicate that the sulfur in VHMS sulfate minerals, for the most part (see discussion of exceptions below), was derived from coeval seawater sulfate.

Table 1 Estimated $\delta^{18}O$ and δD values for VHMS ore fluids

Deposit	Age (Ma)	$\delta^{18}O$ (‰)	δD (‰)	T (°C)	Method of estimation	Source
Active sea floor vents	0.0	1.3 ± 0.9	1 ± 3	220–400	Measurements of venting flids adjusted to remove influence of entrained seawater	DeRonde (1995)
Hokuroku district, Japan		-0.7 ± 1.6	-30 to -10	230–270	Fluid inclusion analysis forδD; quartz$\delta^{18}O$ and fluid inclusion T_h for$\delta^{18}O$	Hattori and Sakai (1979)
Kosaka		1.0 ± 2.0	-30 to 15	220–330	Fluid inclusion analysis for δD; quartz $\delta^{18}O$ and fluid inclusion T_h for $\delta^{18}O$	Pisutha-Arnond and Ohmoto (1983); Hattori and Muehlenbachs (1980)
Iwami, Japan		-2.5 ± 0.9	-55 to -35	230–270	Fluid inclusion analysis for δD; quartz $\delta^{18}O$ and fluid inclusion T_h for $\delta^{18}O$	Hattori and Sakai (1979)
Troodos Ophiolite, Cyprus		0.5 ± 1.0	0 ± 5	350	Quartz and whole-rock analyses, assuming temperature	Heaton and Sheppard (1977)
Buchans, Newfoundland		1.5 ± 3.0	-8 ± 2	240–370	Mineral separate analyses and geothermomtry	Kowalik et al. (1981)
Iberian Pyrite Belt						
Aljustrel		3.3 ± 1.8	-1 to 18	160–270	Mineral separate analysis and geothermometry; the calculated $\delta^{18}O$ values range from 0.0‰ to 5.7‰, with modes at 0.0–1.7‰ and 3.1–5.7‰. The $\delta^{18}O$ value range in the mean ± one standard deviation	Barriga and Kerrich (1984); Munha et al. (1986)
Rio Tinto		0.7 ± 0.7	-5 to 8	210–230	Mineral separate analysis and geothermometry; the calculated $\delta^{18}O$ values range from 0.0‰ to 1.3‰	Munha et al. (1986)
Chanca		0.9	-10 to 0	220	Mineral separate analyses and geothermometry	Munha et al. (1986)
Salgadinho		4.0	-10 to 0	230	Mineral separate analyses and geothermometry	Munha et al. (1986)
Feitas		4.2–5.2		270–315	Quartz $\delta^{18}O$ and fluid inclusion T_h	Inverno et al. (2008)
Neves Corvo		8.3 ± 1.5	-37 to -11	300–400	Mineral separate analyses and geothermometry	Relvas et al. (2006)
Boco, Tasmania, Australia		3.2–5.7		270–360	Pyrophllite $\delta^{18}O$ value and thermal stability of pyrophyllite	Herrmann et al. (2009)
Baiyinchang, China		-5.3 to 3.1		160–280	Quartz $\delta^{18}O$ and fluid inclusion T_h	Hou et al. (2008)
Bruce, Arizona, USA		1.5 ± 0.5		250–300	Extrapolated chlorite value, assuming temperature	Larson (1984)
Crandon, Wisconsin, USA		-0.9 ± 0.8	-15 to 0	220–290	Mineral separate analyses and geothermometry; the calculated $\delta^{18}O$ values range from -2.1‰ to 0.1‰	Munha et al. (1986)

(continued)

Table 1 (continued)

Deposit	Age (Ma)	$\delta^{18}O$ (‰)	δD (‰)	T (°C)	Method of estimation	Source
Mattagami Lake, Quebéc, Canada		1.5 ± 1.0	1 ± 3	240–350	Mineral separate $\delta^{18}O$ and fluid inclusion T_h	Costa et al. (1983)
Noranda district, Quebéc, Canada						
Horne		3.0 ± 1.5	-40 to -30	250–350	Mineral separate analyses and geothermometry	Maclean and Hoy (1991)
Mobrun		2.0 ± 2.0		150–250	Mineral separate analyses and geothermometry	Hoy (1993)
Norbec		1.0 ± 2.0		200–300	Mineral separate analyses and geothermometry	Hoy (1993)
Amulet		0.5 ± 1.0		250–350	Mineral separate analyses and geothermometry	Beaty and Taylor (1982)
Ansil		-0.5 ± 1.0		200–350	Mineral separate analyses and geothermometry	Hoy (1993)
Corbet		-2.0 ± 2.0		250–300	Mineral separate analyses and geothermometry	Hoy (1993)
Kidd Creek, Ontario, Canada		3.8 ± 0.5	-8 ± 5	300–350	Chlorite analyses, assuming temperature	Huston and Taylor (1999)
South Bay, Ontario, Canada		3.3 ± 1.2		300	Quartz analyses, assuming temperature	Urabe and Scott (1983)
Panorama, Western Australia						
VHMS	3240	-0.8 ± 2.6	-48 to -23	90–270	Mineral separate $\delta^{18}O$ and fluid inclusion T_h; fluid inclusion waters and mineral separates for δD	Drieberg et al. (2013)
Granite-hosted veins (greisen)	3240	4.1 to 9.9 (9.3 ± 0.6)	-48 to -18	240–590 (590)	Mineral separate $\delta^{18}O$ and fluid inclusion T_h; fluid inclusion waters and mineral separates for δD	Drieberg et al. (2013)

This is in accord with paragenetic observations and thermodynamic-based models suggesting the sulfate minerals in VHMS deposits form when upwelling hydrothermal fluids mix with sulfate-bearing seawater (cf. Eldridge et al. 1983; Ohmoto et al. 1983).

In contrast, the offset between $\delta^{34}S_{sphalerite}$ and seawater $\delta^{34}S_{seawater\ sulfate}$ in Phanerozoic deposits could be the results of several different processes. For Phanerozoic deposits $\Delta^{34}S_{seawater\ sulfate\text{-}sphalerite}$ ranges from 3‰ to 30‰, with a strong mode at 15–20‰ (median = 19.5‰: Fig. 9c). A similar pattern is seen for $\Delta^{34}S_{sulfate\text{-}sphalerite}$ using data from Phanerozoic deposits for which $\delta^{34}S$ data are available for both sulfate minerals and sphalerite (Fig. 9d). The range in $\Delta^{34}S_{seawater\ sulfate\text{-}sphalerite}$ for Phanerozoic deposits has been explained by several processes, including: (1) biogenic reduction of seawater sulfate (Sangster 1968), (2) derivation of sulfur from a deep-seated (magmatic) source (Ishihara and Sasaki 1978), or (3) partial or complete reduction of seawater sulfate during circulation of evolving seawater (Sasaki 1970; Solomon et al. 1988). A more detailed discussion of these alternatives is presented by Huston (1999), and it is likely that all three, and possibly other, processes have contributed to secular variability in sulfur isotope characteristics of Phanerozoic deposits. It is important to stress that the values used in constructing Figs. 9 and 10 are median values and are indications of the "average" composition of deposits. Some deposits have very large ranges individually, and it is likely that non-hydrothermal processes, such as biogenic processes, have contributed to the variability in $\delta^{34}S_{sulfide}$ in these deposits, particularly at the micro-scale (see below).

The restricted, near-0‰ range of $\delta^{34}S_{sphalerite}$ and near-10‰ range of $\delta^{34}S_{sulfate}$ of Archean deposits, combined with evidence of only minor contributions of seawater sulfur from multiple sulfur isotope studies (see below) suggest that sulfur sources of VHMS deposits early in Earth's history differ from those later in Earth's history. The near-0‰ and, particularly, the uniform character of $\delta^{34}S_{sphalerite}$ in Archean deposits

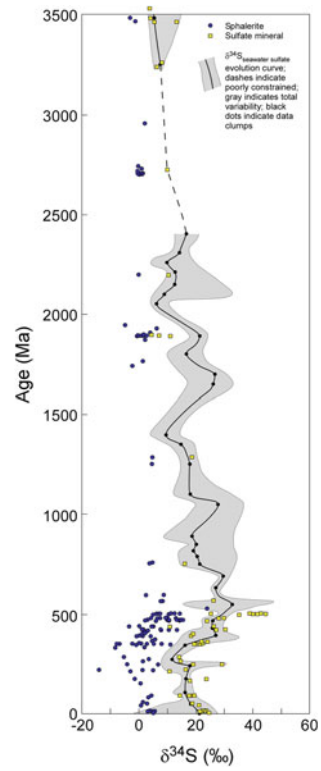

Fig. 10 Variations in $\delta^{34}S$ of sphalerite and sulfate minerals from VHMS deposits through time. Data shown are median values for individual deposits from Huston et al. (2022). Seawater sulfate curve (heavy line with light gray field showing full variability) is based on compilation of Crockford et al. (2019) supplemented by Neo- and Paleoarchean barite data of Huston et al. (2022)

suggests a dominant (leached) igneous origin of sulfide in these deposits.

To test this hypothesis the relative contribution of reduced seawater sulfate versus magmatic sulfur were determined using the median $\delta^{34}S_{sphalerite}$ data (Huston et al. 2022) and the estimated $\delta^{34}S$ of coeval seawater sulfate determined from the $\delta^{34}S_{seawater\ sulfate}$ curve of Claypool et al. (1980) and from a second $\delta^{34}S_{seawater\ sulfate}$ curve determined from evaporite data in Crockford et al. (2019). For periods of time not covered by the respective curves, estimates of $\delta^{34}S_{seawater\ sulfate}$ were made based on $\delta^{34}S_{sulfate}$ of Strauss (2004) and $\delta^{34}S_{barite}$ data from Huston et al. (2022). Numeric values for both curves are tabulated in Huston et al. (2022).

A small proportion of median $\delta^{34}S_{sphalerite}$ values were negative. If the value was between 0‰ and -5‰ (i.e. within the typical range of magmatic sulfur), a $\delta^{34}S_{sphalerite}$ value of 0‰ was assigned to the deposit (n = 17). Deposits with median $\delta^{34}S_{sphalerite}$ values below -5‰ were excluded from the analysis (n = 4).

The deposits were split into three groups by age: Archean (> 2500 Ma), Paleoproterozoic (2500–1600 Ma) and Mesoproterozoic-Phanerozoic (< 1600 Ma). Based on both the Claypool (not shown) and the Crockford (Fig. 11) $\delta^{34}S_{seawater\ sulfate}$ curves, the "typical" contribution (as measured by both median and mean estimates) of reduced seawater sulfate to VHMS sulfur budgets is significantly higher (20–25%) in Mesoproterozoic to Phanerozoic deposits than in Archean deposits (5–10%). The Mesoproterozoic-Phanerozoic distribution is characterized by a strong, tight mode at 0–5%, a much broader mode with a peak at 15–30% and a tail of values up to ~ 75% (Fig. 11a). In contrast, the Archean distribution is characterized by a strong mode with a peak at 0–15% and a tail with values to ~ 25% (Fig. 11d). The Archean distribution is consistent with estimates of seawater sulfate contributions based on multiple sulfur isotope data (0% - Panorama (3238 Ma): Golding et al. 2011; 3% - Kidd Creek (2714 Ma): Jamieson et al. 2013; < 5% - cauldron margin deposits and < 15% main cauldron and post cauldron deposits, Noranda district (2698 Ma): Sharman et al. 2015; 15% - Teutonic Bore and 18% Bentley (2694 Ma); Chen et al. 2015). The data are also consistent with interpretations from multiple sulfur isotope data that Neoarchean seawater contained much lower concentrations of sulfate than modern seawater (80 µmol/l at 2714 Ma versus 28,000 µmol/l presently: Jamieson et al. 2013).

Analysis of the data using the two different $\delta^{34}S_{seawater\ sulfate}$ curves yielded somewhat different results for Paleoproterozoic deposits: both

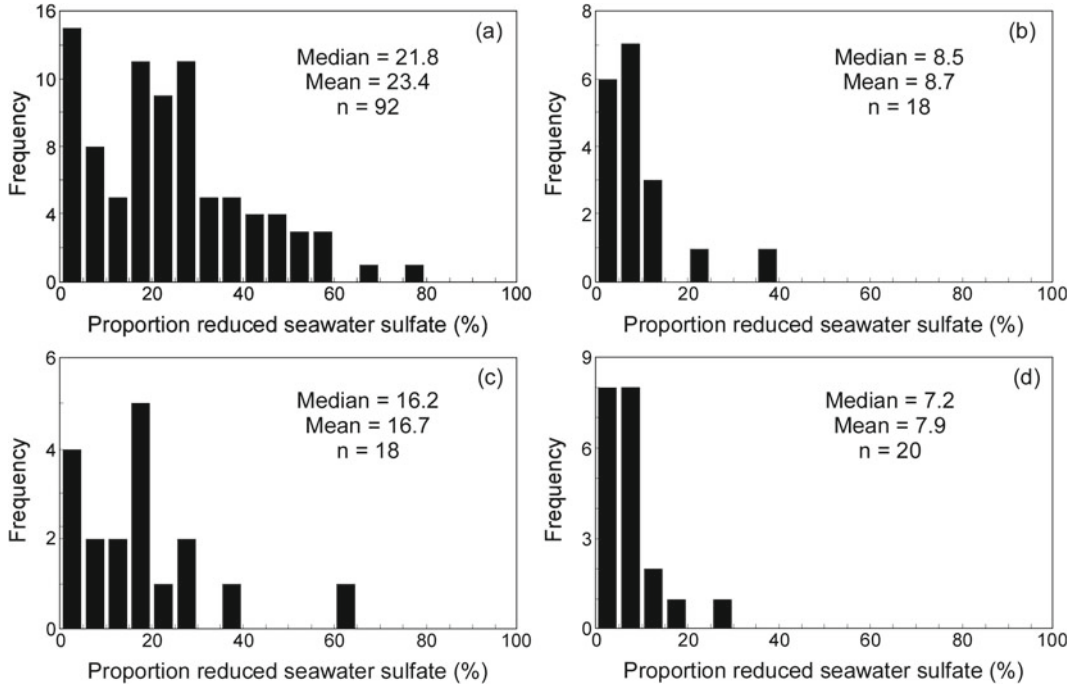

Fig. 11 Histograms showing the estimation contribution of reduced seawater sulfate to sulfur budgets for VHMS deposits that formed during the: (a) Mesoproterozoic to Phanerozoic, (b) and (c) Paleoproterozoic, and (d) Archean. Histogram (b) was calculated using the sulfate data from Crockford et al. (2019) whereas (c) was calculated using Paleoproterozoic barite data from Huston et al. (2022)

indicate a smaller contribution of seawater sulfate than in the Mesoproterozoic-Phanerozoic period, but differed relative to the Archean. Use of the Crockford et al. (2019)-based curve yielded a "typical" seawater sulfate contribution for Paleoproterozoic deposits nearly identical to that of Archean deposits (Fig. 11b), with a major peak at 0–15% and a tail with values to ~ 25%. In contrast use of $\delta^{34}S_{seawater\ sulfate}$ values from ore-related barite yields "typical" seawater sulfate contributions of ~ 16–17% (Fig. 11c). This discrepancy is due to the much higher $\delta^{34}S_{seawater\ sulfate}$ values based on the Crockford et al. (2019) data. A seawater sulfate contribution to the Paleoproterozoic VHMS budget of ~ 16% is consistent with results obtained from the ca 2027 Ma DeGrussa deposit in Western Australia (LaFlamme et al. 2021; see below). This analysis suggests more data are required to better calibrate the Paleoproterozoic (and Meso- to Paleoarchean) $\delta^{34}S_{seawater\ sulfate}$ curve. Analysis is ongoing as to the control of other factors, such as deposit type and alteration assemblage, on the seawater sulfate contributions to the VHMS sulfur budget.

The dominance of a magmatic sulfur source in all ages of deposits does not necessarily imply a magmatic-hydrothermal origin for the sulfur. Rather, given that the host succession of VHMS deposits is generally dominated by volcanic rocks, a more likely source for the sulfur in the deposits is leached sulfur from the underlying volcanic pile, as documented by Brauhart et al. (2001) in the Panorama district, and discussed below. The inference that Paleoproterozoic-Archean VHMS deposits are dominated by leached volcanic sulfur is also consistent with the likely composition of seawater during this time. Holland (1972) originally proposed that Paleoproterozoic and Archean seawater was reduced, iron-rich and sulfate-poor relative to modern seawater. Calculations by Huston (1999) also suggested that Paleoproterozoic-Archean seawater was also sulfide-poor, with H_2S concentrations in the parts per billion range. If Paleoproterozoic-Archean seawater was indeed sulfate- and sulfide-poor, the sulfur source of VHMS deposits would have been dominated by leached volcanic or magmatic sulfide, a conclusion supported by multiple sulfur isotope studies of the Neoarchean Kidd Creek (Jamieson et al. 2013) and Jaguar (Chen et al. 2015) deposits (see also below).

Following a compilation of the occurrence of sulfate minerals in volcanic-hosted massive sulfide deposits, Huston and Logan (2004) observed that Paleoarchean deposits commonly contain sulfate minerals within mineralized zones, whereas Mesoarchean to Paleoproterozoic deposits were rarely sulfate-bearing. A more comprehensive compilation (data from Huston et al. 2022) indicates that 64% (7 out of 11) of Paleoarchean deposits contain sulfate minerals, a higher rate than even Phanerozoic deposits (44%: 232 of 530), and that only 6% (16 of 280) of Neoarchean to Paleoproterozoic deposits contain sulfate minerals. Huston and Logan (2004) interpreted the rare occurrence of sulfate minerals in Neoarchean to Paleoproterozoic deposits as the result of the low concentration of sulfate in reduced seawater of this age, following Holland (1972). In contrast, the common occurrence of sulfate minerals in Phanerozoic deposits is interpreted to be the result of the common presence of sulfate in Phanerozoic oceans, with relatively restricted periods of anoxia (Eastoe and Gustin 1996). The most surprising result of these studies was the common presence of sulfate in Paleoarchean (>3200 Ma) deposits, which was interpreted as the consequence of either a thin sulfate-bearing surficial oceanic layer (c.f. Huston and Logan, 2004) or local concentrations of sulfate caused by volcanic activity. In both cases the sulfate is interpreted to be the consequence of rainout of sulfate produced by photolytic disproportionation of SO_2 in the atmosphere (Farquhar et al. 2000), a hypothesis developed to explain anomalous $\Delta^{33}S$ (see below for definition) signatures of Paleoarchean VHMS sulfates (Golding et al. 2011). The presence of $\Delta^{33}S$ signatures in Neoarchean deposits has also been critical in establishing sulfur sources in these deposits (see below). An unresolved issue is the lack of sulfates in Meso- to Neoarchean deposits as photolytic disproportionation of atmospheric SO_2 is thought to have continued until the Great

Oxidation Event at ~ 2400 Ma (Farquhar et al. 2000, 2013).

4.2.2 Deposit and District-scale Variations in $\delta^{34}S$ from Phanerozoic Deposits

Conventional $\delta^{34}S$ analyses from Phanerozoic VHMS deposits commonly have variabilities of 15‰ or more (e.g., Ducktown, Tennessee: LeHuray 1984; Bathurst, New Brunswick: Goodfellow and Peter 1999; Ming, Newfoundland: Brueckner et al. 2015; Hercules, Tasmania: Khin Zaw and Large 1992). These large ranges most likely reflect the complexities of sulfur sources and geochemical interactions, as discussed above, within the underlying rock pile and at or near the depositional site. Below we describe the $\delta^{34}S$ characteristics of three Phanerozoic provinces, Cambro-Ordovician deposits in the Dunage Zone, Newfoundland, Cambrian deposits in the West Tasmania Terrane, and the Iheya black smoker deposit south of Japan, as well as active seafloor systems in general. These provinces were chosen not only to illustrate $\delta^{34}S$ variability, but to discuss processes that cause the variability.

Deposits in the Dunnage Zone, Newfoundland. Cambro-Ordovician VHMS deposits of the Newfoundland Appalachians occur within volcanic and volcanosedimentary units in the Dunnage Zone (Fig. 12a). This zone hosts numerous VHMS deposits, including Cambrian mafic, bimodal-mafic, bimodal-felsic and felsic-siliciclastic deposits (Kean et al. 1995; Hinchey 2011; Pilote et al. 2014; Cloutier et al. 2015), and Ordovician bimodal-mafic and bimodal-felsic deposits (Dunning et al. 1987; MacLachlan and Dunning 1998). The $\delta^{34}S$ signatures of Dunnage Zone VHMS deposits are highly variable and include data from the Ming ($\delta^{34}S$ = 1–20‰; Brueckner et al. 2015), Whalesback ($\delta^{34}S$ = 1–6‰; Cloutier et al. 2015), Lemarchant ($\delta^{34}S$ = -38 to + 14‰; Lode et al. 2017), and mafic deposits from Notre Dame Bay ($\delta^{34}S$ = 2–20‰; Bachinski 1978; Toman 2013). The characteristics of the Ming and Lemarchant deposits are described in more detail below.

The ~ 487 Ma Ming deposit (21.9 Mt at 1.49% Cu, 0.19% Zn, 3.21 g/t Ag, and 0.61 g/t Au) is spatially associated with boninitic to arc tholeiitic mafic rocks and hosted by tholeiitic felsic rocks the Pacquet Complex in the Baie Verte Peninsula, Newfoundland (Pilote et al. 2017). The deposit contains variably Au-Cu-bearing massive sulfide that is locally capped by a strongly quartz-altered rhyolite, which are together underlain by a footwall zone with Cu-rich chalcopyrite-pyrite-pyrrhotite-chlorite-rich stringers (Brueckner et al. 2015). In situ sulfur isotopic data for pyrite, chalcopyrite, pyrrhotite and arsenopyrite in massive and semi-massive sulfide mineralization have $\delta^{34}S$ between 2.8‰ and 12.0‰, whereas stringer sulfides have $\delta^{34}S$ values of 6‰ to 16‰; sulfides in the quartz-altered rhyolite cap have heavier $\delta^{34}S$ values of 5.9‰ to 19.6‰ (Fig. 12b; Brueckner et al. 2015). Notably, there are decreases in $\delta^{34}S$ of mineral assemblages interpreted to have formed at higher temperatures (e.g., > 300 °C chalcopyrite-pyrrhotite-pyrite assemblages), whereas those forming most proximal to the massive sulfide-seawater interface (e.g., those in the quartz-altered rhyolite cap) have higher $\delta^{34}S$ values (Fig. 12b; Brueckner et al., 2015).

The ca 513–509 Ma Lemarchant deposit is a polymetallic bimodal felsic deposit (2.28 Mt at 0.64% Cu, 9.87% Zn, 1.51% Pb, 99.9 g/t Ag, and 1.26 g/t Au) hosted by felsic rocks of the Bindons Pond formation in the Tally Pond Group (Cloutier et al. 2017). The deposit contains barite, sphalerite, galena, pyrite, and chalcopyrite, as well as abundant sulfosalt minerals, with enrichment in epithermal suite elements (Gill et al. 2016, 2019). The ores are overlain by sulfide-rich hydrothermal mudstones genetically related to mineralization (Cloutier et al. 2017).

Ores and hydrothermal mudstones from Lemarchant have the widest known range in $\delta^{34}S$ for VHMS deposits, ranging from -38.8‰ to 15.1‰ (Lode et al. 2017; Gill et al. 2019). Within the mineralized system, the $\delta^{34}S$ values of pyrite and chalcopyrite (0.3‰ to 10.6‰) overlap with the values for galena (-6.4‰ to 15.1‰: Fig. 12c). In contrast, $\delta^{34}S$ of sulfide

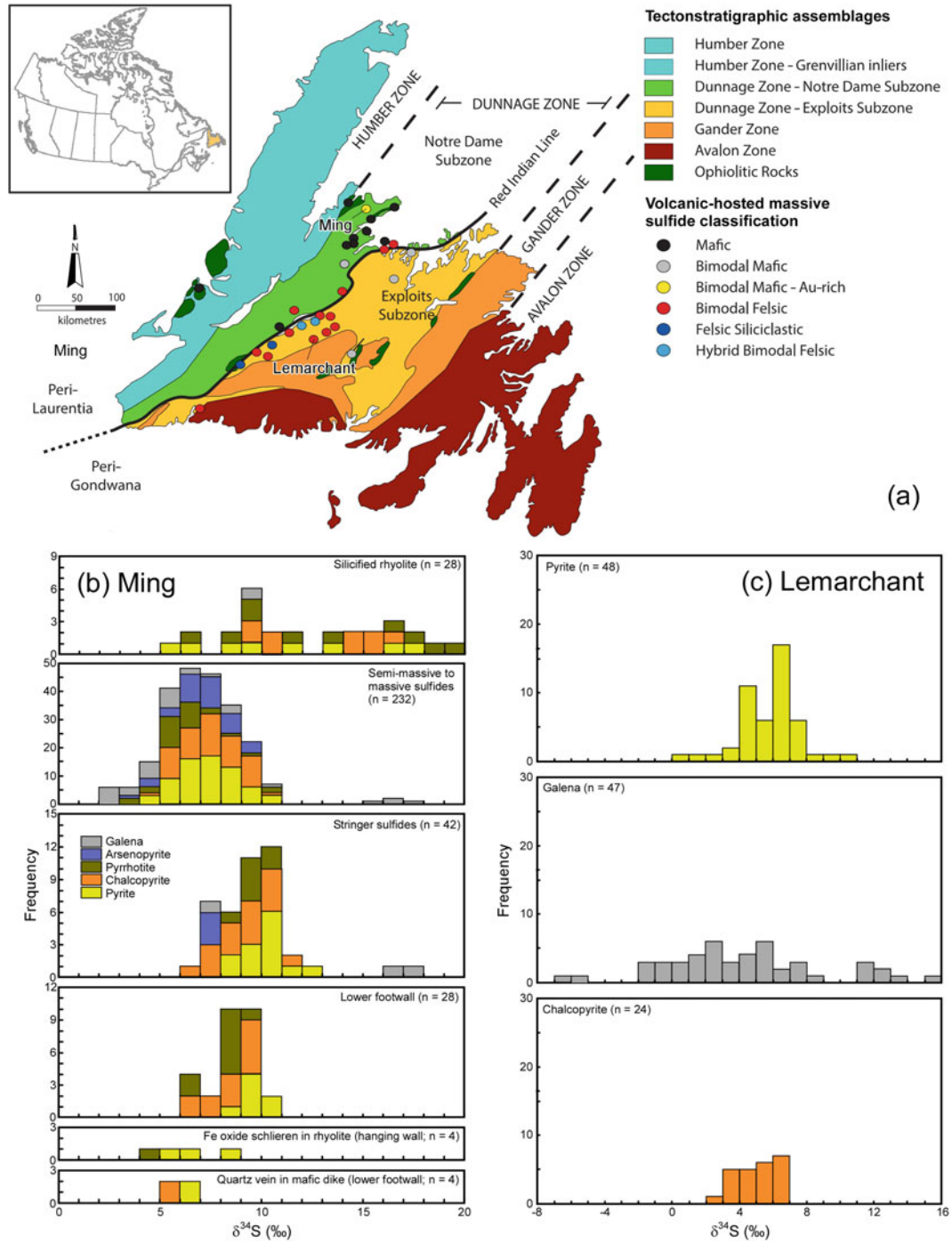

Fig. 12 Sulfur isotope characteristics of volcanic-hosted massive sulfide deposits in the Dunnage Zone, Newfoundland: (a) location of Dunnage Zone and major deposits (modified after Lode et al. 2017), (b) histogram showing the distribution of $\delta^{34}S$ in sulfide minerals from the Ming deposit (modified after Brueckner et al. 2015), (c) histogram showing the distribution of $\delta^{34}S$ in sulfide minerals from the ore zone of the Lemarchant deposit (modified after Gill et al. 2019)

minerals in the hydrothermal mudstones ranges from -38.8 to 14.4‰, with an average value of -12.6‰ (not shown). Proximal to mineralization, however, $\delta^{34}S$ tends to be higher and overlaps values from massive sulfide (Lode et al. 2017).

Overall, these results indicate that the relative proportion of TSR-derived H_2S and leached igneous H_2S (± magmatic-hydrothermal sulfur) from the surrounding host rocks is variable within each deposit. For instance, Brueckner et al. (2015) and Cloutier et al. (2015) showed that the vast majority (>50%) of sulfur in the Ming and Whalesback deposits was from leaching of igneous basement (with a possible contribution of magmatic-hydrothermal sulfur for Ming) with much lesser contributions coming from TSR-derived H_2S, particularly for assemblages that were Cu-rich and/or those with enrichments in epithermal suite elements, including precious metals. Gill et al. (2019) showed that there was H_2S derived from both leaching and TSR in the Lemarchant deposit, but they also argued that some of the low $\delta^{34}S$ values (< 0‰) found were the result of magmatic-hydrothermal SO_2 disproportionation upon cooling and condensing, and the generation of light signatures in sulfides that crystallized incorporated the magmatic-hydrothermal derived H_2S. Mudstones from this same deposit have a much more complex history of biogenic sulfate reduction, microbial sulfide oxidation, and microbial disproportionation of intermediate sulfur compounds; however, with proximity to mineralization $\delta^{34}S$ increased to values near of above 0‰, indicating a greater hydrothermal input and possible magmatic-hydrothermal input. Higher grade copper zones are associated with $\delta^{34}S$ close to 0‰, Zn-Pb-rich zones are often associated $\delta^{34}S$ signatures consistent with mixed igneous and TSR-derived H_2S, whereas deposits enriched in Au, Ag and related elements can have igneous, TSR, or, possibly, magmatic-hydrothermal H_2S with low $\delta^{34}S$ values. These findings highlight the utility of $\delta^{34}S$ of an exploration vector to high grade ore in the VHMS setting, and are discussed further below.

High sulfidation deposits. Sillitoe et al. (1996) observed that a small proportion of VHMS and black smoker deposits contain significant amounts of minerals, such as bornite and tennantite, that are characteristic of hypogene high sulfidation hydrothermal conditions. Many of these deposits are also characterized by hypogene advanced argillic alteration assemblages, defined by the presence of minerals such as kaolinite, pyrophyllite and diaspore. Following work by Gamo et al. (1997), Herzig et al. (1998) and Gemmell et al. (2004), Huston et al. (2011) compared the $\delta^{34}S$ signature of high sulfidation deposits with that of more typical deposits (Fig. 13), for both modern black smokers and Cambrian VHMS deposits in western Tasmania. They found that high sulfidation deposits are characterized anomalously light $\delta^{34}S_{sulfide}$ and $\delta^{34}S_{sulfur}$ signatures, generally between -10‰ and 0‰, which is significantly lower than the $\delta^{34}S$ range seen in coeval deposits that lack high sulfidation mineralogy and advanced argillic alteration assemblages (mostly 0–10‰ for black smoker deposits and 8–19‰ for the western Tasmanian deposits: Fig. 13). Moreover, $\delta^{34}S$ of barite associated with the high sulfidation assemblage in the Tasmanian deposits (19–30‰: Walshe and Solomon 1981) and at Hine Hina (16–17‰: Herzig et al. 1988) are lower than coeval seawater and 20–30‰ heavier than coeval sulfide minerals (i.e. $\Delta^{34}S_{barite\text{-}sulfide} \sim$ 20–30‰).

The sulfur isotope systematics at Hine Hina were interpreted by Herzig et al. (1998) to indicate the incorporation of significant quantities of H_2S produced by disproportionation of magmatic SO_2 to form H_2S and H_2SO_4 and highly acidic hydrothermal fluids. The data from high sulfidation deposits in general can be interpreted similarly, as discussed by Huston et al. (2011), who concluded that "the presence of a major population of anomalously low $\delta^{34}S_{sulfide}$ can be suggestive of disproportionation of magmatic-hydrothermal SO_2, particularly if $\Delta^{34}S_{sulfate\text{-}sulfide} \sim$ 20–30‰, $\Delta^{34}S_{seawater\ sulfate\text{-}ore\ sulfate}$ is non-zero (i.e. $|\Delta^{34}S_{seawater\ sulfate\text{-}ore\ sulfate}| > 5‰$)

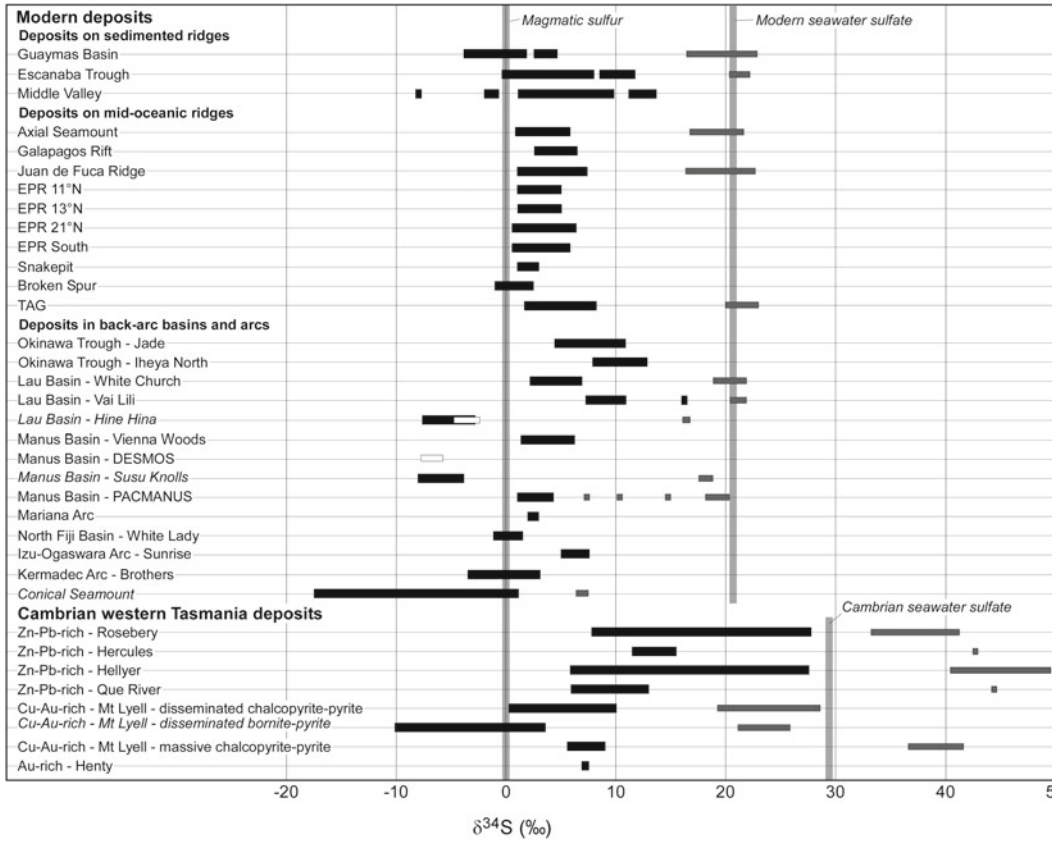

Fig. 13 Comparison of $\delta^{34}S$ values for hydrothermal sites on midocean ridges and arc environments on the modern seafloor and for deposits from the Cambrian Mount Read district, Tasmania. Modified from Herzig et al. (1998) and Gemmell et al. (2004) to include data from Kim et al. (2004), Solomon et al. (1969, 1988), Green et al. (1981) and Walshe and Solomon (1981). Intalicized names indicate high sulfidation deposits

and, most importantly, advanced argillic alteration assemblages are present."

Iheya North black smoker deposit. The Iheya North hydrothermal field (Fig. 14a) is located within the Okinawa Trough, interpreted to be an incipient intracontinental arc-back-arc basin (Shinjo and Kato 2000). Nine hydrothermal mounds make up the field, occurring within bimodal basaltic-rhyolite volcanic rocks, overlain by terrigenous sediments (Ishibashi et al. 2015). The Integrated Ocean Drilling Program Expedition 331 completed 5 drill holes into and surrounding the North Big Chimney (Fig. 14b; shows three of five holes). Sulfur isotope analyses of hydrothermal pyrite in the five drill holes at varying depths demonstrates that the massive sulfides at the North Big Chimney yield consistent $\delta^{34}S = 11.9 \pm 1.1‰$ (1σ: Figs. 14c-d), near identical to the $\delta^{34}S$ composition of the vent fluid (Aoyama et al. 2014). However, progressively outwards from the main vent site hydrothermal pyrite returns lower and more variable $\delta^{34}S$ values of $7.0 \pm 3.8‰$ (1σ) (LaFlamme et al. 2018: Fig. 14e).

The spatial variation within the hydrothermal system indicates that the lower temperature surroundings of the hydrothermal system precipitate hydrothermal pyrite with an increasingly depleted $\delta^{34}S$ value. LaFlamme et al. (2018) demonstrate that this pattern can only be accounted for by way of increased leaching of $\delta^{34}S$-depleted sedimentary pyrite originally deposited by biotic

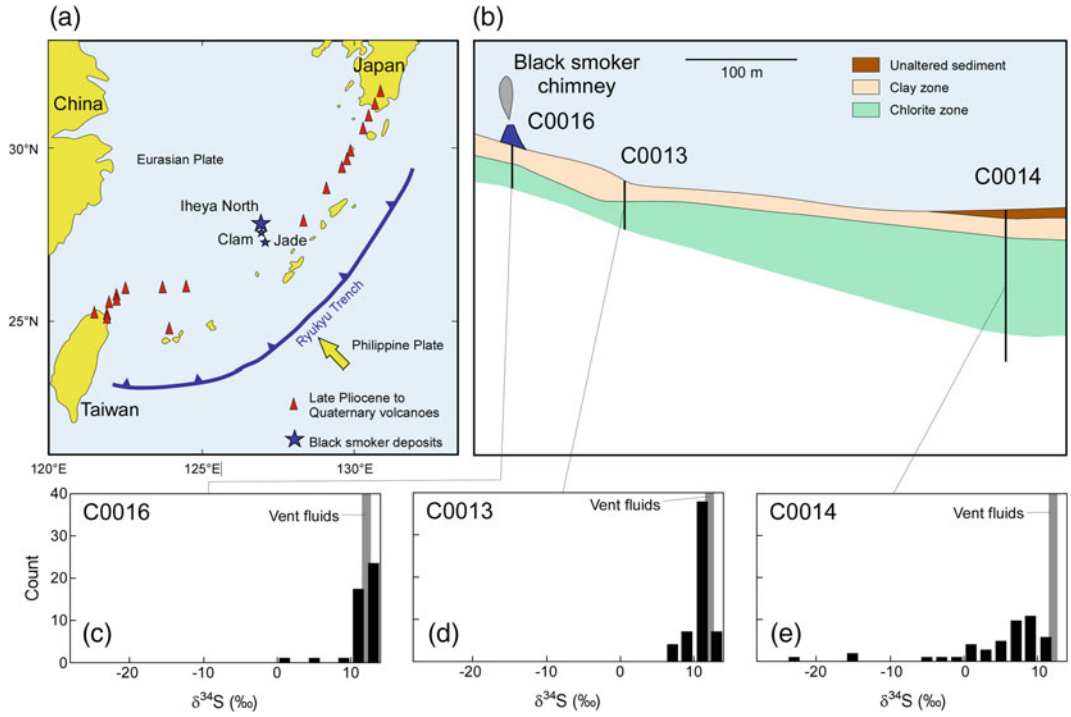

Fig. 14 Diagrams showing (a) the location of the Iheya North black smoker deposit, (b) a geological cross section of the deposit showing the locations of the drill holes, and (c) to (e) $\delta^{34}S$ distributions from the three drill holes showing proximal to distal variations in $\delta^{34}S$ (modified after LaFlamme et al 2018)

metabolisms. As the most significant metal enrichments (Fe, Zn, Cu, Bi, Tl, and Cd) are associated with sulfides at the North Big Chimney containing $\delta^{34}S$ values near-identical to the vent fluid, it is clear that sulfur isotopes can vector toward metals in sedimented seafloor hydrothermal systems (LaFlamme et al. 2018). This knowledge can then be applied in metal vectoring within VHMS deposits.

Modern seafloor systems on divergent margins. Prior to the discovery of seafloor hydrothermal systems along convergent margins in the 1990s, a large amount of data, including $\delta^{34}S$ data of venting fluids and ore minerals, had been collected from seafloor systems on divergent margins (Shanks 2001 and references therein). Although collected from a different tectonic setting, these data provide insights into sulfur sources and processes that cause $\delta^{34}S$ variability in seafloor systems. One of the more puzzling results was the observation that in the 9–10°N East Pacific Rise (9–10°N EPR) vent field, minerals on the inside walls of venting chimneys appear to be out of equilibrium with the venting fluids: $\Delta^{34}S_{\text{vent-inner wall sulfide}} \sim 1.8$–4.0‰, much greater the fractionation expected at the temperatures of venting (Shanks 2001).

Shanks (2001) also indicate that geological events can change isotopic signatures of the vent fluid. Immediately following a seismic (cracking) event at depth in the 9–10°N EPR vent field, $\delta^{34}S$ values of the vent fluid at the P vent decreased sharply by ~ 3‰, coinciding with significant changes in vent chemistry (although not $\delta^{18}O$). Hence it appears that geological events can cause significant changes in the isotopic (and chemical) characteristics of active systems, changes that cannot be documented in ancient systems due to the lack of precise temporal information available for modern systems.

4.2.3 Multiple Sulfur Isotopes

In addition to ^{32}S and ^{34}S, sulfur has two other stable isotopes, ^{33}S and ^{36}S. Although fractionation of the isotopes has been measurable for decades (e.g., Hulston and Thode 1965), ^{33}S and ^{36}S were thought to fractionate relative to ^{32}S (and ^{34}S) in a mass-dependent manner. Farquhar et al. (2000), however, found that, for some reactions, ^{33}S and ^{36}S fractionate independent of mass (mass-independent fractionation or MIF). Farquhar et al. (2000) and subsequent workers (Farquhar and Wing 2003; Johnston et al. 2007) showed that MIF occurs during photolytic breakdown of atmospheric SO_2 restricted to before the Great Oxidation Event (older than ca 2400 Ma). Mass independent fractionations of ^{33}S and ^{36}S are measured by $\Delta^{33}S$ and $\Delta^{36}S$, which indicate deviation from mass-dependent fractionation. These two parameters were defined by Farquhar et al. (2000) and processes that produce MIF are reviewed by Farquhar and Wing (2003), Johnston (2011) and Huston et al. (2023).

Multiple sulfur isotope studies have become important in genetic studies of VHMS deposits, enabling more precise estimates of the relative sulfur inputs from seawater sulfate, sulfur leached from sediments containing pyrite derived by bacterial sulfate reduction, and igneous sulfur in different environments (Ono et al. 2007; Peters et al. 2010; McDermott et al. 2015; Martin et al. 2021), and improving the understanding of the involved in this input. We illustrate uses of multiple sulfur isotopes in VHMS research using three examples, (1) assessment of isotopic and paragenetic equilibrium, (2) assessment of seawater-derived sulfur in Archean deposits, and (3) determination of sulfur sources and mineralizing processes at the DeGrussa deposit, Western Australia.

Assessing isotopic and paragenetic equilibrium. One of the more difficult aspects of interpreting isotopic data is determining if mineral assemblages analyzed are in isotopic equilibrium. If this can be established, isotopic fractionation between minerals can be used to estimate the temperature of mineral crystallization and the isotopic composition of the ore fluid. Typically, this is determined based on paragenetic relationships: if the minerals are in textural equilibrium, it is assumed that they are in isotopic equilibrium. Paragenetic relations, however, are not always straightforward and can be controversial; moreover, they can be overprinted or destroyed by later recrystallization. Jamieson et al. (2006) presented a method of independently assessing isotopic (dis)equilibrium using $\delta^{34}S$ and $\Delta^{33}S$ data in Archean rocks. These authors took advantage of the fact that $\Delta^{33}S$ is not changed by mass dependent fractionation; during equilibrium fractionation between two minerals, $\delta^{34}S$ fractionates but $\Delta^{33}S$ remains constant. Hence, if two minerals have statistically different $\Delta^{33}S$, it is unlikely that they are in isotopic equilibrium. Conversely, similar $\Delta^{33}S$ values are consistent with isotopic equilibrium, although crystallization from two different fluids with similar $\Delta^{33}S$ would also appear to be in isotopic equilibrium. Jamieson et al. (2006) used this method to assess eight mineral pairs from the Kidd Creek deposit. Two mineral pairs were not considered to be in isotopic equilibria, and a further three were considered to be in equilibria but small fractionation factors between the two minerals precluded the calculation of meaningful temperatures. One of the mineral pairs interpreted to be out of isotopic equilibrium from the $\Delta^{33}S$ data was clearly out of equilibrium from the $\delta^{34}S$ data. The three remaining mineral pairs in apparent isotopic equilibria yielded depositional temperatures within the expected ranges, consistent with being in true isotopic equilibrium. Although this technique is time restricted largely to the Archean, it provides independent criteria for assessing isotopic (dis)equilibria. The method is also applicable to assessing in situ data collected using secondary ion mass spectrometry (SIMS: Whitehouse 2013).

Sulfur sources in Archean deposits. In the Archean, prior to significant fractionation in $\delta^{34}S$ of VHMS deposits, the $\Delta^{33}S$ record of these deposits has proven to be useful (e.g., Jamieson et al. 2013; Caruso et al. 2019). At that time, the ferruginous ocean chemistry reflected the low redox state of the atmosphere and ocean basins incorporated atmosphere-derived elemental sulfur and sulfate formed by mass independent

fractionation of sulfur (MIF-S) with large positive and negative $\Delta^{33}S$ anomalies (> ± 0.2‰; Farquhar et al. 2013). Therefore, the recycling of sulfur derived from the Archean ocean seawater sulfate may be traced using this signature. Neoarchean VHMS deposits, including the Kidd Creek (Jamieson et al. 2013) and Noranda (Sharman et al. 2015) deposits of the Superior Craton, as well as the Teutonic Bore complex (Chen et al. 2015) and Nimbus deposits (Caruso et al. 2019) of the Yilgarn Craton, generally preserve $\Delta^{33}S < 0$‰. This predominantly negative $\Delta^{33}S$ signature is interpreted to indicate hydrothermal fluids incorporated a small component of Archean seawater sulfate (3–18%), which recycled the oxidised form of MIF-S. Barré et al. (2022) suggested that in the Noranda and Matagami districts of the Abitibi Subprovince multiple sulfur isotope signatures can be directly correlated with metal endowment of deposits. Massive Zn-Cu-sulfide sub-seafloor replacement deposits incorporate less seawater sulfate and preserve a near igneous signature, whereas less-endowed Fe-exhalites yield a higher proportion of seawater sulfate and an increasingly enriched $\delta^{34}S$ and depleted $\Delta^{33}S$ signature, reflecting the isotopic composition of the Archean ocean seawater sulfate reservoir. Exhalites are intimately linked to massive sulfide occurrences, and so their sulfur isotope composition may be utilised for within-camp targeting.

DeGrussa deposit, Western Australia. The ~ 2.03 Ga DeGrussa Cu-Au–Ag deposit (and satellite Monty deposit) is located in the Bryah Basin of the Paleoproterozoic Capricorn Orogen of Western Australia (Hawke et al. 2015: Fig. 15). The deposits contain 9 Mt at 4.5% Cu and 1.5 g/t gold (Hilliard et al. 2017). Massive sulfide ore lenses are associated with gabbroic sills that intrude tubiditic volcaniclastic rocks, interpreted to have formed in a continental rift setting (Occhipinti et al. 2017). Massive sulfide ore lenses are commonly associated with magnetite and consist of pyrite with lesser pyrrhotite and chalcopyrite (LaFlamme et al. 2021).

An integrated dataset of in situ multiple sulfur isotope data and conventional fluorination-IRMS multiple sulfur isotope analyses identifies an overprinting non-VHMS sulfide mineralizing event with $\delta^{34}S > 8$‰. The original VHMS mineralizing event at Degrussa, however, yields $\delta^{34}S$ from 2.9‰ to 3.6‰, and $\Delta^{33}S$ from -0.08‰ to 0.00‰. A two component $\delta^{34}S$-$\Delta^{33}S$ mixing model indicates 11% of H_2S is derived from thermochemically reduced seawater sulfate mixed with magmatic H_2S, either derived from leaching of volcanic rock or from magmatic-hydrothermal fluids.

4.2.4 Application of Sulfur Isotope Geochemistry to Exploration and Ore Genesis

Volcanosedimentary basins commonly contain a range of sulfide accumulations (Fig. 16), some related to VHMS mineral systems (e.g., VHMS deposits and exhalites) and some not (e.g., pyritic black shale). Even among VHMS-related accumulations, sulfur sources are diverse, with the source potentially having implications to fertility. As presented above, sulfur isotope data can aid in distinguishing the origin and sulfur source of sulfide accumulations.

An important potential application of sulfur isotopes in VHMS exploration is to distinguish Fe-sulfide accumulations formed solely through sedimentary or diagenetic processes or through metamorphic processes from those that included exhalative hydrothermal sulfur (Brueckner et al. 2015; Lode et al. 2017; LaFlamme et al. 2021). Sulfur isotope characteristics, based on our review and shown in Fig. 16, appear to be sufficiently distinctive to distinguish exhalative components and may allow vectoring once exhalative horizons are determined.

Once a VHMS-related hydrothermal occurrence has been identified, sulfur isotope data may aid potential assessment and ranking during exploration programs. Different parts of a VHMS mineral system may have distinctive $\delta^{34}S$ signatures due to the varying incorporation of sulfur from different sources through the system (Fig. 16). The massive sulfide and stringer zones, produced by deposition of hydrothermal sulfide

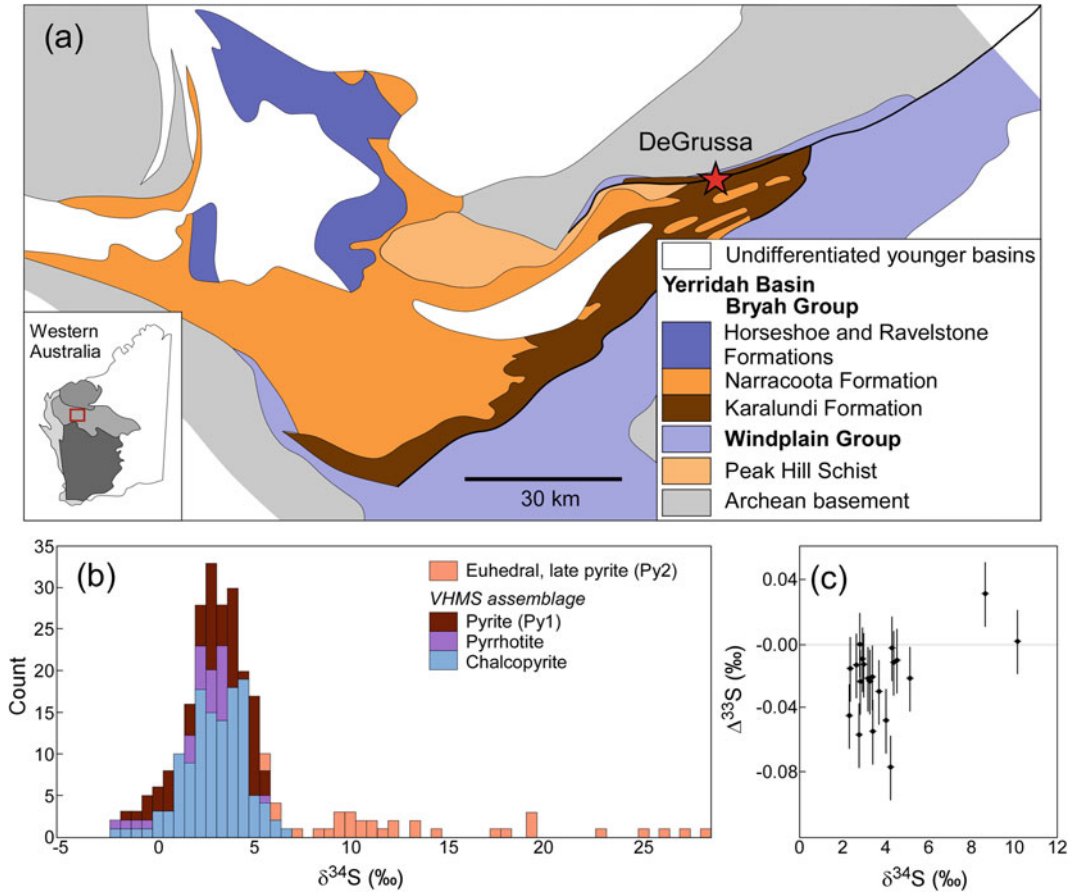

Fig. 15 Diagrams showing (a) the location and regional geology of the DeGrussa deposit, (b) a histogram showing variations in in situ $\delta^{34}S$ analyses of sulfide minerals, and (c) a scattergram showing the relationship between $\delta^{34}S$ and $\Delta^{33}S$ using fluorination analysis. Reproduced with permission and with small modification from LaFlamme et al. (2021); Copyright 2021 Elsevier

at or below the seafloor, have $\delta^{34}S$ signatures that reflect varying proportions of sulfide produced by thermochemical sulfate reduction of seawater sulfate ($\delta^{34}S \sim \delta^{34}S_{coeval\ seawater\ sulfate}$), leached from igneous sulfur deep in the VHMS system ($\delta^{34}S \sim 0‰$) or generated by disproportionation of magmatic SO_2 ($\delta^{34}S \sim$ -15‰ to -5‰). During early-stage prospect evaluation and near-mine exploration, these signatures may assist in discriminating the genesis and potential of prospects or new lens: for example, a significant population ore minerals with $\delta^{34}S$ below 0‰ may indicate the presence of Cu-Au-rich high sulfidation potential, particularly if accompanied by advanced argillic alteration assemblages ore an ore assemblage enriched in metals such as Bi, Te, Mo, Sn and Se..

A second tracer in sulfur isotope space, $\Delta^{33}S$, can further elucidate seawater contribution of sulfur to the system, especially in Precambrian deposits, in which the conventional seawater sulfur isotope signature is less certain (see LaFlamme et al. 2021). Mixing models in $\delta^{34}S$-$\Delta^{33}S$ space, can better predict the multiple sulfur isotope signature of massive sulfide ore. Preliminary work has highlighted that at the district scale, $\delta^{34}S$- $\Delta^{33}S$ signature of massive sulfide ore lenses may be directly correlated to Au grade (Sharman et al. 2015). Therefore, more studies concentrated on the potential of near-mine

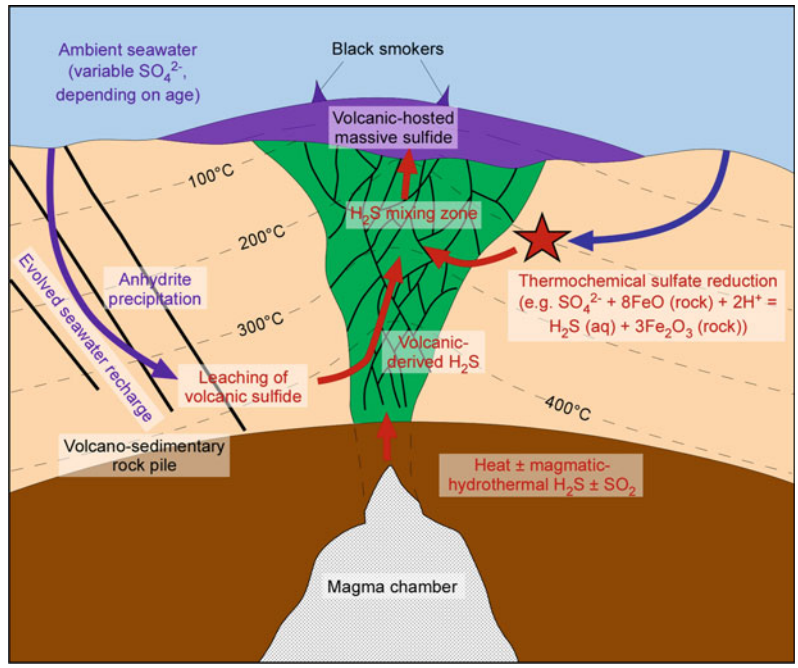

Fig. 16 Model of a seafloor hydrothermal system (not to scale) showing sulfur sources and sinks, and reactions involving that occur during fluid circulation below and on the seafloor (modified after LaFlamme et al. 2021)

multiple sulfur isotope vectoring within VHMS deposits of various ages and tectonic setting are warranted.

5 Application of and Impediments to the Use of Light Stable Isotopes in Exploration

Although stable isotope studies have been critical to characterizing and understanding ore-forming processes in VHMS systems, they have not been extensively utilized by the exploration industry, largely because of the slow turn-around time and high costs relative to other analytical tools. The review above has suggested that there are isotopic patterns that are potentially useful for exploration at the district to deposit scale. Further, the development of in-situ methods at relatively reasonable cost and with high volume analysis, compared to conventional methods, suggests the potential for more widespread usage with continued analytical development into the future.

The only example where isotopic data has been directly used to discover a VHMS deposit is the study by Miller et al. (2001), who combined whole rock oxygen isotope with other geochemical data to map paleothermal gradients and discover the West 45 lens at the ~ 480 Ma Thalanga deposit, Queensland. This illustrates the utility of whole rock oxygen isotope data at the deposit scale, and studies such as those by Cathles (1993) and Brauhart et al. (2000) illustrate the potential use of whole rock oxygen isotope data at the district scale.

6 Conclusions and Future Directions

Since recognition of VHMS deposits as a class, light stable isotopes, particularly those of oxygen, hydrogen and sulfur, have played a key role in understanding the hydrothermal system that formed these deposits. Estimates of fluid oxygen and hydrogen isotope data, determined from mineral isotopic data, suggest that in most cases evolved seawater was the dominant hydrothermal fluid. There is, however, sound evidence that magmatic-hydrothermal contributions may be important in some VHMS deposits, particularly when isotopic data are supported by other

indicators of magmatic-hydrothermal input such as certain alteration assemblages and enrichment in particular elements. These latter deposits can be important as they can be enriched in metals such as tin, gold and other elements associated with magmatic-hydrothermal contributions. Alteration associated with hydrothermal flow leaves consistent patterns in whole rock oxygen isotope data that can be used to define fluid flow pathways, both at the deposit and district scales. When combined with whole rock geochemical or mineralogical data, the isotopic data can be used to produce paleotemperature maps.

Sulfur isotope data also provide important insights into the VHMS system, particularly addressing the sources of sulfur. Conventional $\delta^{34}S$ and multiple isotope data (e.g., $\Delta^{33}S$ data) indicate that although reduced seawater sulfate has been a component of the sulfur budget of VHMS systems since the Paleoarchean, its importance has increased in general from 5–10% in the Archean to 15–20% in the Paleoproterozoic and to 20–25% in the Phanerozoic; within these time intervals, however, the proportion can vary significantly between deposits. The other component is magmatic sulfur, which can be derived by leaching of volcanic rocks or through input of magmatic-hydrothermal H_2S or SO_2. The latter may be important to form high sulfidation VHMS deposits (c.f. Sillitoe et al. 1996), which are commonly enriched in gold.

Possibly because of their relatively high cost and/or slow turn-around time, isotopic data have not been employed extensively in exploring for VHMS deposits. Despite this, oxygen isotopes have directly contributed to the discovery of a new ore lens at the Thalanga deposit in Queensland (Miller et al. 2001), and they clearly have potential to produce paleotemperature and fluid flow maps at the deposit and district scales. Sulfur isotope data have utility in fingerprinting mineralized from barren sulfide bodies, and may also provide vectors to ore.

The last twenty years has seen many significant improvements in analytical technologies and in the understanding of stable isotope systematics. The most important has been the development of microanalytical tools such as LA-ICP-MS that allow rapid in situ isotopic analysis of petrographically constrained samples. Moreover, rapid and inexpensive analytical techniques are being developed for a range of light stable isotopic systems (see Huston et al. 2023 for discussion) that may allow the rapid collection of large datasets useful in exploration.

The other major leap has come through the use of multiple isotopic systems such as the oxygen and, as discussed here, the sulfur system. Prior to 2000, ^{33}S and ^{36}S were rarely analyzed and largely ignored. The discovery of mass-independent sulfur isotope fractionation has resulted in major changes in our understanding of the sulfur cycle and new insights into ancient environments on Earth. These discoveries have also impacted our understanding of VHMS systems, including evidence of the importance of reduced seawater sulfate even before the Great Oxidation Event.

New technologies and the understanding derived from them will continue to impact our understanding of the VHMS mineral system. These new isotopic data will lead to new discoveries, either directly as costs come down, or indirectly, through better understanding of mineralizing processes.

Acknowledgements The authors thank David Champion, Jens Gutzmer and an anonymous reviewer, for their reviews that have significantly improved this contribution. This contribution is published with permission of the Chief Executive Officer of Geoscience Australia.

References

Addy SK, Ypma PJM (1977) Origin of massive sulfide deposits at Ducktown, Tennessee: an oxygen, carbon and hydrogen isotope study. Econ Geol 72:1245–1268

Aggarwal PK, Longstaffe FJ (1987) Oxygen-isotope geochemistry of metamorphosed massive sulfide deposits of Flin Flon—Snow Lake belt, Manitoba. Contrib Mineral Petrol 96:314–325

Aoyama S, Nishizawa M, Katai K, Ueno Y (2014) Microbial sulfate reduction within the Iheya North subseafloor hydrothermal system constrained by

quadruple sulfur isotopes. Earth Planet Sci Lett 398:113–126. https://doi.org/10.1016/j.epsl.2014.04.039

Aruajo SM, Scott SD, Longstaffe FJ (1996) Oxygen isotope composition of alteration zones of highly metamorphosed volcanogenic massive sulfide deposits; Geco, Canada, and Palmeiropolis, Brazil. Econ Geol 91:697–712

Bachinski DJ (1978) Sulfur isotopic composition of thermally metamorphosed cupriferous iron sulfide ores associated with cordierite-anthophyllite rocks, Gull Pond, Newfoundland. Econ Geol 73:64–72

Barré G, LaFlamme C, Beaudoin G, Goutier J, Cartigny P (2022) The application of multiple sulphur isotopes to determine the architecture of Archean VMS deposits. Geol Assoc Can-Mineral Assoc Can Abstr 45:50

Barrie CT, Hannington MD (1999) Classification of VMS deposits based on host rock composition. Rev Econ Geol 8:1–12

Barriga FJAS, Kerrich R (1984) Extreme ^{18}O-enriched volcanics and ^{18}O-evolved marine water, Aljustrel, Iberian Pyrite Belt: transition from high to low Rayleigh number convective regimes. Geochim Cosmochim Acta 48:1021–1031

Beaty DW, Taylor HP Jr (1982) Some petrologic and oxygen isotope relationships in the Amulet mine, Noranda, Quebec, and their bearing on the origin of Archean massive sulfide deposits. Econ Geol 77:95–108

Beaty DW, Taylor HP Jr, Coads PR (1988) An oxygen isotope study of the Kidd Creek, Ontario, volcanogenic massive sulfide deposit: evidence for a high ^{18}O ore fluid. Econ Geol 83:1–17

Beaudoin G, Mercier-Langevin P, Dube B, Taylor BE (2014) Low-temperature alteration at the world-class LaRonde Penna Archean Au-rich volcanogenic massive sulfide deposit, Abitibi Subprovince, Quebec, Canada: evidence from wholerock oxygen isotopes. Econ Geol:167–182

Blevin PL, Chappell BW (1995) Chemistry, origin, and evolution of mineralized granites in the Lachlan fold belt, Australia: the metallogeny of I- and S-type granites. Econ Geol 90:1604–1619

Brauhart CW, Groves DI, Morant P (1998) Regional alteration systems associated with volcanogenic massive sulfide mineralization at Panorama, Pilbara, Western Australia. Econ Geol 93:292–302

Brauhart CW, Huston DL, Andrew A (2000) Definition of regional alteration in the Panorama VMS district using oxygen isotope mapping: implications for the origin of the hydrothermal system and applications to exploration. Mineral Deposita 35:727–740

Brauhart CW, Huston DL, Groves DI, Mikucki EJ, Gardoll SJ (2001) Geochemical mass transfer patterns as indicators of the architecture of a complete volcanic-hosted massive sulfide hydrothermal alteration system in the Panorama district, Pilbara, Western Australia. Econ Geol 96:1263–1278

Brueckner S, Piercey S, Layne G, Piercey G, Sylvester P (2015) Variations of sulphur isotope signatures in sulphides from the metamorphosed Ming Cu(−Au) volcanogenic massive sulphide deposit, Newfoundland Appalachians, Canada. Mineral Deposita 50:619–640

Buick R, Brauhart CW, Morant P, Thornett JR, Maniw J, Archibald NJ, Doepel M (2002) Geochronology and stratigraphic relationships of the Sulphur Springs Group and Strelley Granite: a temporally distinct igneous province in the Archaean Pilbara craton, Australia. Precambrian Res 114:87–120

Caruso S, Fiorentini ML, Barnes SJ, LaFlamme C, Martin LA (2019) Microchemical and sulfur isotope constraints on the magmatic and hydrothermal evolution of the Black Swan Succession, Western Australia. Mineral Deposita 317:211–229

Cathles LM (1993) Oxygen isotope alteration in the Noranda mining district, Abitibi greenstone belt, Quebec. Econ Geol 88:1483–1511

Chaussidon M, Albarede F, Sheppard SMF (1989) Sulphur isotope variations in the mantle from ion microprobe analyses of micro-sulphide inclusions. Earth Planet Sci Lett 92:144–156

Chen M, Campbell IH, Xue Y, Tian W, Ireland TR, Holden P, Cas RAF, Hayman PC, Das R (2015) Multiple sulfur isotope analyses support a magmatic model for the volcanogenic massive sulfide deposits of the Teutonic Bore Volcanic Complex, Yilgarn Craton, Western Australia. Econ Geol 110:1411–1423

Claypool GE, Holser WT, Kaplan IR, Sakai H, Zak I (1980) The age curves of sulfur and oxygen isotopes in marine sulfate and their mutual interpretation. Chem Geol 28:199–260

Cloutier J, Piercey SJ, Layne G, Heslop J, Hussey A, Piercey G (2015) Styles, textural evolution, and sulfur isotope systematics of Cu-rich sulfides from the Cambrian Whalesback volcanogenic massive sulfide deposit, central Newfoundland, Canada. Econ Geol 110:1215–1234

Cloutier J, Piercey SJ, Lode S, Vande Guchte M, Copeland DA (2017) Lithostratigraphic and structural reconstruction of the Zn-Pb-Cu-Ag-Au Lemarchant volcanogenic massive sulphide (VMS) deposit, Tally Pond group, central Newfoundland, Canada. Ore Geol Rev 84:154–173

Converse DR, Holland HD, Edmond JM (1984) Flow rates in the axial hot springs of the East Pacific Rise (21°N): implications for the heat budgets and the formation of massive sulfide deposits: Earth Planet Sci Lett 69:159–175

Costa UR, Barnett RL, Kerrich R (1983) The Mattagami Lake mine Archean Zn-Cu sulfide deposit, Quebec: hydrothermal coprecipitation of talc and sulfides in a sea-floor brine pool—evidence from geochemistry, ^{18}O/^{16}O, and mineral chemistry. Econ Geol 78:1144–1203

Crockford PW, Kunzmann M, Bekker A, Hayles J, Bao H, Halverson GP, Peng Y, Bui TH, Cox GM, Gibson TM, Wörndle S, Rainbird R, Lepland A, Swanson-Hysell NL, Master S, Sreenivas B, Kuznetsov A, Krupenik V, Wing BA (2019) Claypool

continued: extending the isotopic record of sedimentary sulfate. Chem Geol 513:200–225
Date J, Watanabe Y, Saeki Y (1983) Zonal alteration around the Fukazawa kuroko deposits, Akita Prefecture, northern Japan. Econ Geol Mon 5:365–386
de Groot PA (1993) Stable isotope (C, O, H), major- and trace element studies on hydrothermal alteration and related ore mineralization in the volcano-sedimentary belt of Bergslagen, Sweden. Geologica Ultraiectina, 98, 181 pp
de Ronde CEJ (1995) Fluid chemistry and isotope characteristics of seafloor hydrothermal systems and associated VMS deposits: potential for magmatic contributions. Mineral Assoc Can Short Course Ser 23:479–509
Ding T, Valkiers S, Kipphardt H, De Bièvre P, Taylor PDP, Gonfiantini R, Krouse R (2001) Calibrated sulfur isotope abundance ratios of three IAEA sulfur isotope reference materials and V-CDT with a reassessment of the atomic weight of sulfur. Geochim Cosmochim Acta 65:2433–2437
Doyle MG, Allen RL (2003) Subsea-floor replacement in volcanic-hosted massive sulfide deposits. Ore Geol Rev 23:183–222
Drieberg SL, Hagemann SG, Huston DL, Landis G, Ryan CG, Van Achterbergh E, Vennemann T (2013) The interplay of evolved seawater and magmatic-hydrothermal fluids in the 3.24 Ga Panorama volcanic-hosted massive sulfide hydrothermal system, north Pilbara Craton. Western Australia. Econ Geol 108:79–110
Dubé B, Gosselin P, Mercier-Langevin P, Hannington M, Galley A (2007) Gold-rich volcanogenic massive sulphide deposits. Mineral Deposits Division, Geol Assoc Can Spec Publ 5:75–94
Dunning GR, Kean BF, Thurlow JG, Swinden HS (1987) Geochronology of the Buchans, Roberts Arm, and Victoria Lake groups and Mansfield Cove Complex, Newfoundland. Can J Earth Sci 24:1175–1184
Eastoe CJ, Gustin MM (1996) Volcanogenic massive sulfide deposits and anoxia in the Phanerozoic oceans. Ore Geol Rev 10:179–197
Eldridge CS, Barton PB, Ohmoto H (1983) Mineral textures and their bearing on formation of the Kuroko orebodies. Econ Geol Mon 5:241–281
Farquhar J, Bao H, Thiemens M (2000) Atmospheric influence of Earth's earliest sulfur cycle. Science 28:756–758
Farquhar J, Cliff J, Zerkle AL, Kamyshyn A, Poulton SW, Adams CM, Harms DB (2013) Pathways for Neoarchean pyrite formation constrained by mass-independent sulfur isotopes. Proc National Acad Sci 110:17638–17643
Farquhar J, Wing BA (2003) Multiple sulfur isotopes and the evolution of the atmosphere. Earth Planet Sci Let 213:1–13
Franklin JM, Lydon JW, Sangster DM (1981) Volcanic-associated massive sulfide deposits. Econ Geol 75th Anniv Vol, pp 485–627
Franklin JM, Gibson HL, Jonasson IR, Galley AG (2005) Volcanogenic massive sulfide deposits. Econ Geol 100th Anniv Vol, pp 523–560
Friedman I., O'Neil JR (1977) Compilation of stable isotope fractionation factors of geochemical interest. US Geol Surv Prof Pap 440-KK:1–12
Galley AG (2003) Composite synvolcanic intrusions associated with Precambrian VMS-related hydrothermal systems. Mineral Deposita 38:443–473
Gamo T, Okamura K, Charlou J, Urabe T, Auzende J, Ishibashi J, Shitashima K, Chiba H, Binns RA, Gena K, Henry K, Matsubayashi O, Moss R, Nagaya Y, Naka J, Ruellan E (1997) Acidic and sulfate-rich hydrothermal fluids from the Manus back-arc basin, Papua New Guinea. Geology 25:139–142
Gemmell JB, Sharpe R, Jonasson I, Herzig P (2004) Sulfur isotope evidence for magmatic contribution to subaqueous and subaerial epithermal mineralisation: Conical Seamount and Ladolam Au deposit, Papua New Guinea. Econ Geol 99:1711–1725
Gill SB, Piercey SJ, Layton-Matthews D (2016) Mineralogy and metal zoning of the Cambrian Zn-Pb-Cu-Ag-Au Lemarchant volcanogenic massive sulfide (VMS) deposit, Newfoundland. Can Mineral 54:1307–1344
Gill SB, Piercey SJ, Layne GD, Piercey G (2019) Sulphur and lead isotope geochemistry of sulphide minerals from the Zn-Pb-Cu-Ag-Au Lemarchant volcanogenic massive sulphide (VMS) deposit, Newfoundland, Canada. Ore Geol Rev 104:422–435
Golding SD, Duck LJ, Young E, Baublys KA, Glikson M, Kamber BS (2011) Earliest seafloor hydrothermal systems on Earth: comparisons with modern analogues. In: Golding SD, Glikson M (eds) Earliest life on Earth: habitats, environments and methods of detection. Springer, Dordrecht, pp 15–49
Goodfellow W, Peter J (1999) Sulphur isotope composition of the Brunswick No. 12 massive sulphide deposit, Bathurst Mining Camp, New Brunswick: implications for ambient environment, sulphur source, and ore genesis. Can J Earth Sci 36:127–134
Green GJ, Taheri J (1992) Stable isotopes and geochemistry as exploration indicators. Bull Geol Surv Tasmania 70:84–91
Green GR, Solomon M, Walshe JL (1981) The formation of the volcanic-hosted massive sulfide at Rosebery, Tasmania. Econ Geol 76:304–338
Green GR, Ohmoto H, Date J, Takahashi T (1983) Whole-rock oxygen isotope distribution in the Fukazawa-Kosaka area, Hokuroku district, Japan, and its potential application to mineral exploration. Econ Geol Mon 5:395–411
Hagemann S, Hensler A-S, Figueiredo e Silva RC, Tsiko H (2023) Light stable isotope (O, H, C) signatures of BIF-hosted iron ore systems: implications for genetic models and exploration targeting. In : Huston DL, Gutzmer J (eds) Isotopoes in economic geology, meallogenesis and exploration, Springer, Berlin, this volume

Hannington MD, de Ronde CEJ, Petersen S (2005) Seafloor tectonics and submarine hydrothermal systems. Econ Geol 100th Anniv Vol, pp 111–141

Hannington M, Jamieson J, Monecke T, Petersen S, Beaulieu S (2011) The abundance of seafloor massive sulfide deposits. Geology 39:1155–1158

Hart H, Gibson HL, Lesher CM (2004) Trace element geochemistry and petrogenesis of felsic volcanic rocks associated with volcanogenic Cu–Zn–Pb massive sulfide deposits. Econ Geol 99:1003–1013

Hattori K, Muehlenbachs K (1980) Marine hydrothermal alteration at a kuroko deposit, Kosaka, Japan. Contrib Mineral Petrol 74:285–292

Hattori K, Sakai H (1979) D/H ratios, origins, and evolution of the ore-forming fluids for the Neogene veins and kuroko deposits of Japan. Econ Geol 74:535–555

Hawke ML, Meffre S, Stein H, Hilliard P, Large R, Gemmell B (2015) Geochronology of the DeGrussa volcanic-hosted massive sulfide deposit and associated mineralisation of the Yerrida, Bryah and Padbury basins, Western Australia. Precambrian Res 267:250–284

Heaton THE, Sheppard SMF (1977) Hydrogen and oxygen isotope evidence for sea-water-hydrothermal alteration and ore deposition, Troodos complex, Cyprus. Volcanic processes in ore genesis. Institute of Mining and Metallurgy, London, pp 42–57

Herrmann W, Green GR, Barton MD, Davidson GJ (2009) Lithogeochemical and stable isotopic insights into submarine genesis of pyrophyllite-altered facies at the Boco prospect, western Tasmania. Econ Geol 104:775–792

Herzig PM, Hannington MD (1995) Polymetallic massive sulfides at the modern seafloor. a review. Ore Geol Rev 10:95–115

Herzig PM, Hannington MD, Arribas A Jr (1998) Sulfur isotope composition of hydrothermal precipitates from the Lau back-arc: implications for magmatic contributions to seafloor hydrothermal systems. Mineral Deposita 33:226–237

Hilliard P, Adamczyk KE, Hawke ML (2017) DeGrussa copper-gold deposit. Austr Inst Mining Metall Mon 32:393–400

Hinchey JG (2011) The Tulks volcanic belt, Victoria Lake Supergroup, central Newfoundland – geology, tectonic setting, and volcanogenic massive sulfide mineralization. Nfld Labrador Dep Nat Res Geol Surv St. John's NL Can Rep 2011–02, 167 p

Holk GJ, Taylor BE, Galley AG (2008) Oxygen isotope mapping of the Archean Sturgeon Lake caldera complex and VMS-related hydrothermal system, Northwestern Ontario, Canada. Mineral Deposita 43:623–640

Holland HD (1972) The geologic history of sea water—an attempt to solve the problem. Geochim Cosmochim Acta 36:637–651

Hou Z, Zaw K, Rona P (2008) Geology, fluid inclusions, and oxygen isotope geochemistry of the Baiyinchang pipe-style volcanic-hosted massive sulfide Cu deposit in Gansu Province, northwestern China. Econ Geol 103:269–292

Hoy LD (1993) Regional evolution of hydrothermal fluids in the Noranda district, Quebec: evidence for $\delta^{18}O$ values from volcanogenic massive sulfide deposits. Econ Geol 88:1526–1541

Hulston JR, Thode HG (1965) Variations in the S33, S34, and S36 contents of meteorites and their relation to chemical and nuclear effects. J Geophys Res 70:3475–3484

Huston DL (1999) Stable isotopes and their significance for understanding the genesis of volcanic-hosted massive sulfide deposits: a review. Rev Econ Geol 10:151–180

Huston DL, Logan GA (2004) Barite, BIFs and bugs: evidence for the evolution of the Earth's early hydrosphere. Earth Planet Sci Lett 220:41–55

Huston DL, Taylor BE (1999) Genetic significance of oxygen and hydrogen isotope variations at the Kidd Creek volcanic-hosted massive sulphide deposit, Ontario, Canada. Econ Geol Mon 10:335–350

Huston DL, Stevens B, Southgate PN, Muhling P, Wyborn L (2006) Australian Zn–Pb–Ag ore-forming systems: a review and analysis. Econ Geol 101:1117–1158

Huston DL, Pehrsson S, Eglington BM, Zaw K (2010) The geology and metallogeny of volcanic-hosted massive sulfide deposits: variations through geologic time and with tectonic setting. Econ Geol 105:571–591

Huston DL, Relvas JMRS, Gemmell JB, Drieberg S (2011) The role of granites in volcanic-hosted massive sulphide ore-forming systems: an assessment of magmatic–hydrothermal contributions. Mineral Deposita 46:473–507

Huston DL, Eglington B, Pehrsson S, Piercey SJ (2022) Global database of zinc-lead-bearing mineral deposits. Geosci Austr Rec 2022/10

Huston DL, Trumbull RB, Beaudoin G, Ireland T (2023) Light stable isotopes (H, B, C, O and S) in ore studies —methods, theory, applications and uncertainties. In : Huston DL, Gutzmer J (eds) Isotopoes in economic geology, meallogenesis and exploration, Springer, Berlin, this volume

Hutchinson RW (1973) Volcanogenic sulfide deposits and their metallogenic significance. Econ Geol 68:1223–1246

Inverno CMC, Solomon M, Barton MD, Foden J (2008) The Cu-stockwork and massive sulfide ore of the Feitais volcanic-hosted massive sulfifide deposit, Iberian Pyrite Belt, Portugal: a mineralogical, fluid inclusion, and isotopic investigation. Econ Geol 103:241–267

Ishibashi J-I, Ikegami F, Tsuji T, Urabe T (2015) Hydrothermal activity in the Okinawa Trough backarc basin: geological background and hydrothermal mineralisation. In: Ishibashi J-I (ed) Subseafloor biosphere linked to hydrothermal systems. Springer, Berlin, pp 337–359

Ishihara S, Sasaki A (1978) Sulfur of kuroko deposits—a deep seated origin. Mining Geol 28:361–367

Jamieson JW, Wing BA, Hannington MD, Farquhar J (2006) Evaluating isotopic equilibrium among sulfide

mineral pairs in Archean ore deposits: case study from the Kidd Creek VMS deposit, Ontario, Canada. Econ Geol 101:1055–1061

Jamieson JW, Wing BA, Farquhar J, Hannington MD (2013) Neoarchaean seawater sulphate concentrations from sulphur isotopes in massive sulfide ore. Nature Geosci 6:61–64

Johnston DT (2011) Multiple sulfur isotopes and the evolution of Earth's surface sulfur cycle. Earth-Sci Rev 106:161–183

Johnston DT, Farquhar J, Canfield DE (2007) Sulfur isotope insights into microbial sulfate reduction: when microbes meet models. Geochim Cosmochim Acta 71:3929–3947

Kean BF, Evans DTW, Jenner GA (1995) Geology and mineralization of the Lushs Bight Group, Geol Surv Nfld Labrador Mineral Dev Div St John's NL Can Rep 95–2, 204 p

Keenan JH, Keyes FG, Hill PG, Moore JG (1969) Steam tables—thermodynamic properties of water including vapor, liquid, and solid phases (international edition—metric units). Wiley, New York, p 162

Kerr DJ, Gibson HL (1993) A comparison of the Horne volcanogenic massive sulfide deposit and intracauldron deposits of the Mine Sequence, Noranda, Quebec. Econ Geol 88:1419–1442

Kerrich R, Wyman D (1997) Review of developments in trace-element fingerprinting of geodynamic settings and their implications for mineral exploration. Austr J Earth Sci 44:465–488

Zaw K, Large RR (1992) The precious metal-rich South Hercules mineralization, western Tasmania: a possible subsea-floor replacement volcanic-hosted massive sulfide deposit. Econ Geol 87:931–952

Kim J, Lee I, Lee K-Y (2004) S, Sr, and Pb isotopic systematics of hydrothermal chimney precipitates from the eastern Manus Basin, western Pacific: evaluation of magmatic contribution of hydrothermal system. J Geophys Res 109:B12210

Knauth LP, Beeunus MA (1986) Isotope geochemistry of fluid inclusions in Permian halite with implications for the isotopic history of ocean water and the origin of saline formation waters. Geochim Cosmochim Acta 50:419–433

Kowalik J, Rye RO, Sawkins FJ (1981) Stable-isotope study of the Buchans, Newfoundland, polymetallic sulphide deposits. Geol Assoc Can Spec Pap 22:229–254

LaFlamme C, Hollis S, Jamieson J, Fiorentini M (2018) Three-dimensional spatially-constrained sulfur isotopes highlight processes controlling sulfur cycling in the near surface of the Iheya North hydrothermal system, Okinawa Trough. Geochem Geophys Geosys 19:2798–2812

LaFlamme C, Barré G, Fiorentini ML, Beaudoin G, Occhipinti S, Bell J (2021) A significant seawater sulfate reservoir at 2.0 Ga determined from multiple sulfur isotope analyses of the Paleoproterozoic Degrussa Cu-Au volcanogenic massive sulfide deposit. Geochim Cosmochim Acta 295:178–193

Large RR (1977) Chemical evolution and zonation of massive sulfide deposits in volcanic terrains. Econ Geol 72:549–572

Larson PB (1984) Geochemistry of the alteration pipe at the Bruce Cu-Zn volcanogenic massive sulfide deposit, Arizona. Econ Geol 79:1880–1896

Lerouge C, Deschamps Y, Joubert M, Bechu E, Fouillac AM, Castro JA (2001) Regional oxygen isotope systematics of felsic volcanics; a potential exploration tool for volcanogenic massive sulphide deposits in the Iberian Pyrite Belt. J Geochem Explor 72:193–210

LeHuray AP (1984) Lead and sulfur isotopes and a model for the origin of the Ducktown deposit, Tennessee. Econ Geol 79:1561–1573

Lesher CM, Goodwin AM, Campbell IH, Gorton MP (1986) Trace element geochemistry of ore-associated and barren, felsic metavolcanic rocks in the Superior Province, Canada. Can J Earth Sci 23:222–237

Leybourne MI, Peter JM, Kidder JA, Layton-Matthews D, Petrus JA, Rissmann CFW, Voinot A, Bowell R, Kyser TK (2022) Stable and radiogenic isotopes in the exploration for volcanogenic massive sulfide deposits. Can Mineral 60:433–468

Lode S, Piercey SJ, Layne GD, Piercey G, Cloutier J (2017) Multiple sulphur and lead sources recorded in hydrothermal exhalites associated with the Lemarchant volcanogenic massive sulphide deposit, central Newfoundland, Canada. Mineral Deposita 52:205–128

Lydon JW (1988) Ore deposit models #14. Volcanogenic massive sulphide deposits Part 2: Genetic models. Geosci Can 15:43–65

MacLachlan K, Dunning G (1998) U-Pb ages and tectono-magmatic evolution of Middle Ordovician volcanic rocks of the Wild Bight Group, Newfoundland Appalachians. Can J Earth Sci 35:998–1017

MacLean WH, Hoy LD (1991) Geochemistry of hydrothermally altered rocks at the Horne mine, Noranda, Quebec. Econ Geol 86:506–528

Martin AJ, McDonald I, Jenkin GRT, McFall KA, Boyce AJ, Jamieson JW (2021) A missing link between ancient and active mafic-hosted seafloor hydrothermal systems – magmatic volatile influx in the exceptionally preserved Mala VMS deposit, Troodos. Cyprus. Chem Geol 567:120127

McDermott JM, Ono S, Tivey MK, Seewald JS, Shanks WC III, Solow AR (2015) Identification of sulfur sources and isotopic equilibria in submarine hot-springs using multiple sulfur isotopes. Geochim Cosmochim Acta 160:169–187

Mercier-Langevin P, Dubé B, Hannington MD, Davis DW, Lafrance B, Gosselin G (2007) The LaRonde Penna Au-rich volcanogenic massive sulfide deposit, Abitibi Greenstone Belt, Quebec: Part I. Geology and Geochronology. Econ Geol 102:585–609

Mercier-Langevin P, Caté A, Ross P-S (2014) Whole-rock oxygen isotope mapping, Lalor auriferous VMS deposit footwall alteration zones, Snow Lake, west-central Manitoba (NTS 63K16). Report of Activities 2014, Manitoba Geological Survey, pp 94–103

Miller C, Halley S, Green G, Jones M (2001) Discovery of the West 45 volcanic-hosted massive sulfide deposit using oxygen isotopes and REE geochemistry. Econ Geol 96:1227–1237

Munhá J, Barriga FJAS, Kerrich R (1986) High ^{18}O ore-forming fluids in volcanic-hosted base metal massive sulfide deposits: geologic, $^{18}O/^{16}O$, and D/H evidence from the Iberian Pyrite Belt; Crandon, Wisconsin; and Blue Hill, Maine. Econ Geol 81:530–552

Occhipinti S, Hocking R, Lindsay M, Aitken A, Copp I, Jones J, Sheppard S, Pirajno F, Metelka V (2017) Paleoproterozoic basin development on the northern Yilgarn Craton, Western Australia. Precambrian Res 300:121–140

Ohmoto H (1986) Stable isotope geochemistry of ore deposits. Rev Mineral 16:491–559

Ohmoto H (1996) Formation of volcanogenic massive sulfide deposits: the kuroko perspective. Ore Geol Rev 10:135–177

Ohmoto H, Rye D (1979) Isotopes of sulfur and carbon. In: Barnes HL (ed) Geochemistry of hydrothermal ore deposits, 2nd edn. Wiley, New York, pp 509–567

Ohmoto H, Mizukami M, Drummond SE, Eldridge CS, Pisutha-Arnond V, Lenagh TC (1983) Chemical processes in Kuroko formation. Econ Geol Mon 5:570–604

Ono S, Shanks WC, Rouxel OJ, Rumble D (2007) S-33 constraints on the seawater sulfate contribution in modern seafloor hydrothermal vent sulfides. Geochim Cosmochim Acta 71:1170–1182

Paradis S, Taylor BE, Watkinson DH, Jonasson IR (1993) Oxygen isotope zonation and alteration in the northern Noranda district, Quebec: evidence for hydrothermal fluid flow. Econ Geol 88:1512–1525

Peter JM (2003) Ancient iron formations: their genesis and use in the exploration for stratiform base metal sulphide deposits, with examples from the Bathurst Mining Camp. Geotext 4:145–176

Peters M, Strauss H, Farquhar J, Ockert C, Eickmann B, Jost CL (2010) Sulfur cycling at the Mid-Atlantic Ridge: a multiple sulfur isotope approach. Chem Geol 268:180–196

Petersen S, Lehmann B, Murton BJ (2018) Modern seafloor hydrothermal systems: new perspective on ancient ore-forming processes. Elements 14:307–312

Piercey SJ (2011) The setting, style, and role of magmatism in the formation of volcanogenic massive sulfide deposits. Mineral Deposita 46:449–471

Pilote J-L, Piercey SJ, Mercier-Langevin P (2014) Stratigraphy and hydrothermal alteration of the Ming Cu-Au volcanogenic massive-sulphide deposit, Baie Verte Peninsula, Newfoundland. Geol Surv Can Curr Res 2014–7, 21 pp

Pilote J-L, Piercey SJ, Mercier-Langevin P (2017) Volcanic and structural reconstruction of the deformed and metamorphosed Ming volcanogenic massive sulfide deposit, Canada: implications for ore zone geometry and metal distribution. Econ Geol 112:1305–1332

Pisutha-Arnond V, Ohmoto H (1983) Thermal history, and chemical and isotopic compositions of the ore-forming fluids responsible for the kuroko massive sulfide deposits in the Hokuroku district of Japan. Econ Geol Mon 5:523–558

Quesnel B, Scheffer C, Beaudoin G (2023) The light stable isotope (H, B, C, N, O, Si, S) composition of orogenic gold deposits. In: Huston DL, Gutzmer J (eds) Isotopes in economic geology, metallogenesis and exploration, Springer, Berlin, this volume

Relvas JMRS, Barriga FJAS, Longstaffe F (2006) Hydrothermal alteration and mineralization in the Neves-Corvo volcanic-hosted massive sulfide deposit, Portugal: II. Oxygen, hydrogen and carbon isotopes. Econ Geol 101:791–804

Riverin G, Hodgson CJ (1980) Wall-rock alteration at the Millenbach Cu-Zn mine, Noranda, Quebec. Econ Geol 75:424–444

Rye RO, Bethke PM, Wasserman MD (1992) The stable isotope geochemistry of acid sulfate alteration. Econ Geol 87:225–262

Sangster DF (1968) Relative sulphur isotope abundances of ancient seas and strata-bound sulphide deposits. Proc Geol Assoc Can 19:79–91

Sangster DF, Scott SD (1976) Precambrian stratabound, massive Cu-Z-Pb sulfide ores of North America. In: Wolf KH (ed) Handbook of strata-bound and stratiform ore deposits. Elsevier, Amsterdam, pp 129–222

Sasaki A (1970) Seawater sulfate as a possible determinant for sulfur isotopic compositions of some strata-bound sulfide ores. Geochem J 4:41–51

Shanks WC III (2001) Stable isotopes in seafloor hydrothermal systems: vent fluids, hydrothermal deposits, hydrothermal alteration, and microbial processes. Rev Mineral Geochem 43:469–526

Shanks WC III (2014) Stable isotope geochemistry of mineral deposits. Treatise Geochem, 2nd edn 13:59–85. https://doi.org/10.1016/B978-0-08-095975-7.01103-7

Sharman ER, Taylor BE, Minarik WG, Dubé B, Wing BA (2015) Sulfur isotope and trace element data from ore sulfides in the Noranda district (Abitibi, Canada): implications for volcanogenic massive sulfide deposit genesis. Mineral Deposita 50:591–606

Sheppard SMF (1986) Characterization and isotopic variations in natural waters. Rev Mineral 16:165–183

Shinjo R, Kato Y (2000) Geochemical constraints on the origin of bimodal magmatism at the Okinawa Trough, an incipient backarc basin. Lithos 54:117–137. https://doi.org/10.1016/S0024-4937(00)00034-7

Sillitoe RH, Hannington MD, Thompson JFH (1996) High sulfidation deposits in the volcanogenic massive sulfide environment. Econ Geol 91:204–212

Solomon M, Rafter TA, Jensen ML (1969) Isotope studies on the Rosebery, Mount Farrell and Mount Lyell ores, Tasmania. Mineral Deposita 4:172–199

Solomon M, Eastoe CJ, Walshe JL, Green GR (1988) Mineral deposits and sulfur isotope abundances in the Mount Read Volcanics between Que River and Mount Darwin. Econ Geol 83:1307–1328

Stein CA (1995) Heat flow and hydrothermal circulation. Geophys Mon 91:425–445

Strauss H (2004) 4 Ga of seawater evolution: evidence from the sulfur isotopic composition of sulfate. Geol Soc Am Spec Pap 379:195–205

Taylor BE (1987) Stable isotope geochemistry of ore-forming fluids. Mineral Assoc Can Short Course Ser 13:337–445

Taylor BE (1992) Degassing of H_2O from rhyolitic magma during eruption and shallow intrusion, and the isotopic composition of magmatic water in hydrothermal systems. Geol Surv Jpn Rep 279:190–194

Taylor BE, Holk GJ (2002) Stable applications in the exploration for volcanic-associated massive sulphide deposits: a preliminary summary. Geol Surv Can Open File 4431:41–44

Taylor BE, Huston DL (1999) Regional ^{18}O zoning and hydrogen isotope studies in the Kidd Creek Volcanic Complex, Timmins, Ontario. Econ Geol Mon 10:351–378

Taylor HP Jr, Sheppard SMF (1986) Igneous rocks: I. Processes of isotopic fractionation and isotope systematics. Rev Mineral 16:227–272

Taylor BE, South BC (1985) Regional stable isotope systematics of hydrothermal alteration and massive sulfide deposition in the West Shasta district, California. Econ Geol 80:2149–2163

Taylor BE, Timbal A (2002) Regional stable isotope studies in the Noranda Volcanic. Geol Surv Can Open File 4431:243–252

Taylor BE, de Kemp E, Grunsky E, Martin L, Rigg D, Goutier J, Lauzière K, Dubé B (2014) 3-D visualization of the Archean Horne and Quemont Au-bearing VMS hydrothermal systems, Blake River Group, Québec. Econ Geol 109:183–203

Taylor BE, Peter JM, Laakso K, Rivard B (2015) Oxygen isotope zonation about the Izok Ag-VMS deposit, Slave Province, Nunavut: hanging-wall vector to mineralization. Geol Surv Can Open File 7853:27–44

Toman H (2013) Geology and metallogeny of north-central Newfoundland and the Little Deer VMS deposit. Unpublished M.Sc. thesis, Memorial University of Newfoundland, 184 p

Urabe T, Scott SD (1983) Geology and footwall alteration of the South Bay massive sulphide deposit, northwestern Ontario, Canada. Can J Earth Sci 20:1862–1879

Urabe T, Scott SD, Hattori K (1983) A comparison of footwall-rock alteration and geothermal systems beneath some Japanese and Canadian volcanogenic massive sulfide deposits. Econ Geol Mon 5:345–364

Walshe JL, Solomon M (1981) An investigation into the environment of formation and the volcanic-hosted Mt. Lyell copper deposits using geology, mineralogy, stable isotopes, and a six-component chlorite solid solution model. Econ Geol 76:246–284

Werner RA, Brand WA (2001) Referencing strategies and techniques in stable isotope ratio analysis. Rapid Commun Mass Spectrom 15:501–519

Whitehouse MJ (2013) Multiple sulfur isotope determination by SIMS: evaluation of reference sulfides for $\Delta^{33}S$ with observations and a case study on the determination of $\Delta^{36}S$. Geostand Geoanal Res 37:19–33

Williams N (2023) Stable isotope studies of the clastic-dominated lead-zinc (CD Pb-Zn) mineralization and their implications for ore genesis and exploration. In : Huston DL, Gutzmer J (eds) Isotopoes in economic geology, meallogenesis and exploration, Springer, Berlin, this volume

Zheng Y, Gu L, Tang XQ, Liu SH (2011) Oxygen isotope characteristics of the footwall alteration zones in the Hongtoushan volcanogenic massive sulfide deposit, Liaoning Province, China and restoration of their formation temperatures. Acta Geol Sin 85:683–693

Zierenberg RA, Shanks WC III (1988) Isotopic studies of epigenetic features in metalliferous sediment, Atlantis II Deep, Red Sea. Can Mineral 26:737–753